Title
Overcoming the Limitations of Mineral Scaling and Feed Pressure in Reverse Osmosis Desalination

Author
Kim, Yeunha

Publication Date
2020

Peer reviewed|Thesis/dissertation

UNIVERSITY OF CALIFORNIA

Los Angeles

Overcoming the Limitations of Mineral Scaling and Feed Pressure in Reverse Osmosis Desalination

A thesis submitted in partial satisfaction
of the requirements for the degree of Master of Science
in Chemical Engineering

by

Yeunha Kim

2020

ABSTRACT OF THE THESIS

Overcoming the Limitations of Mineral Scaling
and Feed Pressure in Reverse Osmosis Desalination

by
Yeunha Kim

Master of Science in Chemical Engineering
University of California, Los Angeles, 2020
Professor Yoram Cohen, Chair

Reverse osmosis (RO) membrane desalination is increasingly used for production of potable water from seawater and brackish water and in municipal and industrial water reuse applications. However, RO processes at high recovery are impacted by membrane mineral scaling and the upper pressure barrier of RO elements, pumps and the associated energy expenditure. Membrane surface scaling decreases membrane water permeability and may reduce membrane lifetime. Membrane mineral scaling can be partially mitigated via antiscalant dosing of the RO feed, but this is at an added cost. An alternate approach to scale mitigation can be achieved via RO Feed flow reversal (FFR) which is a chemical-free method. By periodically reversing the direction of the raw RO feed, mineral scale that develops at the membrane stage exit can be removed via dissolution, thereby restoring the membrane permeability. Accordingly, an evaluation of the FFR process in a spiral-wound RO pilot system was carried out, without antiscalant dosing, with gypsum as a model scalant whereby the efficacy of the process was monitored via real time membrane surface monitoring.

The recovery of RO process depends on both the ability to mitigate scaling and overcoming the pressure barrier, particularly for highly saline source water. However, the upper pressure limit constraint on membrane elements and the added energy cost often place a practical limit on the achievable recovery. In order to overcome the pressure limitation, the present work explored the deployment of a hybrid RO-NF configuration. In this arrangement the RO membrane enable balancing the rejection of the target mineral salts while the NF membranes allow for further concentration of the RO concentrate, which is particularly beneficial for source water high in concentration of divalent ions. The NF membrane permeate is then recycled and directed to the RO membranes. The attained recovery range and energy utilization for the above process were explored demonstrating that a higher recovery can be attained at a lower applied pressure relative to conventional RO system configuration.

The thesis of Yeunha Kim is approved.

Panagiotis D. Christofides

Vasilios Manousiouthakis

Yoram Cohen, Committee Chair

University of California, Los Angeles

2020

TABLE OF CONTENTS

LIST OF FIGURES

LIST OF TABLES

ACKNOWLEDGEMENTS

First of all, I sincerely appreciate the guidance and support from the best advisor and mentor I could ask for, Professor Yoram Cohen. I would also like to express my gratitude to Dr. Anditya Rahardianto for offering experienced advice during the experiments. It was truly a pleasure to work with the people in my research group. Especially, the contributions of Anditya Rahardianto, Tae Lee, Yian Chen, and Alex Nosrat are acknowledged in building the pilot RO plant. Lastly, I would like to thank my friends and family for their love, prayers, and support for my academic pursuits.

The research projects described in this thesis were funded, in part, by the Electric Power Research Institute (EPRI), and the Desalination and Water Purification Research Program (DWPR) of the United States Bureau of Reclamation (USBR). I also appreciate the RO and NF membranes provided by Toray/CSM.

1. Introduction

Growing population requires increased water resources that include utilization of non-traditional water sources that often require treatment and salinity reduction. In California, for example, severe drought in 2014 resulted in about 6.6 million acre-foot reduction in surface water for agriculture, $810 million losses in crop revenue, and $203 million losses in livestock and dairy value [1]. In the midst of the drought groundwater provided nearly half of urban and agricultural water supply [2]. Given that natural groundwater is recharge is often insufficient in arid and semi-arid regions, groundwater replenishment via injection of treated reclaimed wastewater has been advanced in various regions in California and around the globe. For example, the Groundwater Replenishment System (GWRS) by Orange County Water District and Orange County Sanitation District system utilizes RO desalination to purify local and imported wastewater and then recharge groundwater. In the San Joaquin Valley [3] groundwater salinity is rising and approaches to salinity reduction are needed and where RO desalination has been explored as a viable solution to salinity reduction. Although RO desalination is now a mature technology, membrane mineral scaling is an impediment that constraints the upper product water recovery that can be attained. Mineral scaling of RO membranes reduces the permeability and shortens the lifetime of RO membranes [3,4]. Moreover, the operating pressure limitation of membrane elements and energy cost for pressurized RO operation [5,6] also impose both an operational and technical constraints, respectively, on the deployment of RO desalination.

There are several methods to mitigate mineral scaling, for example, antiscalant dosing of the RO feed [7], pH adjustment to increase the solubility of sparingly soluble mineral salts whose solubility if pH-dependent (e.g., Calcium carbonate; [8]), and periodic membrane cleaning (including chemical cleaning in place (CIP)). An alternate approach that does not require treatment

chemicals is based on an operation that periodically switches from normal feed flow (NFF) to reversed flow through the RO elements. In this approach, after a period of operation the direction of flow in the RO train is reversed whereby the tail element become the lead elements. When the raw feed water is undersaturated with respect to the mineral scalants of concern, this feed flow reversal (FFR) allow for dissolution removal of scale formed in the tail element in the NFF mode of operation. Previous work at UCLA [9] has shown that there is merit in using the approach. However, the questions that remain are whether the approach can be effective for source water of high scaling propensity and if periodic freshwater flush can improve the overall approach. In order to evaluate the above an experimental investigation was carried out with a pilot RO system capable of operation in which the feed flow direction is periodically reversed.

In addition to the limitation on RO recovery due to mineral scaling, RO membranes have an upper pressure rating for their effective utilization. This pressure barrier imposes limit on the maximum attainable RO recovery which then limits the attainable RO process productivity. A potential approach to overcoming the pressure limitation is to utilize a hybrid RO-NF configuration. RO-NF configuration utilizes RO membranes followed by NF membranes. This process configuration can lower the operating pressure while maintaining the same recovery of a conventional RO configuration. Accordingly, in the present work, both process analysis and experiments were carried out to evaluate the above hypothesis.

2. Background

2.1. Basics of RO Desalination

Reverse Osmosis (RO) is a water desalination process that utilize a semi-permeable membrane to remove solutes. The typical RO membrane is a thin film composite consisting of a 100-200 nm thick polyamide layer on top of a ~40 um polysulfone layer and ~120 um polyester fabric layer [10]. The RO membrane allows the passage of water molecules but rejects solutes and particles with diameters larger than 0.1 nm, including bacteria, viruses, multivalent and monovalent ions. The schematic drawing of a typical RO membrane is shown in Figure 2.1.

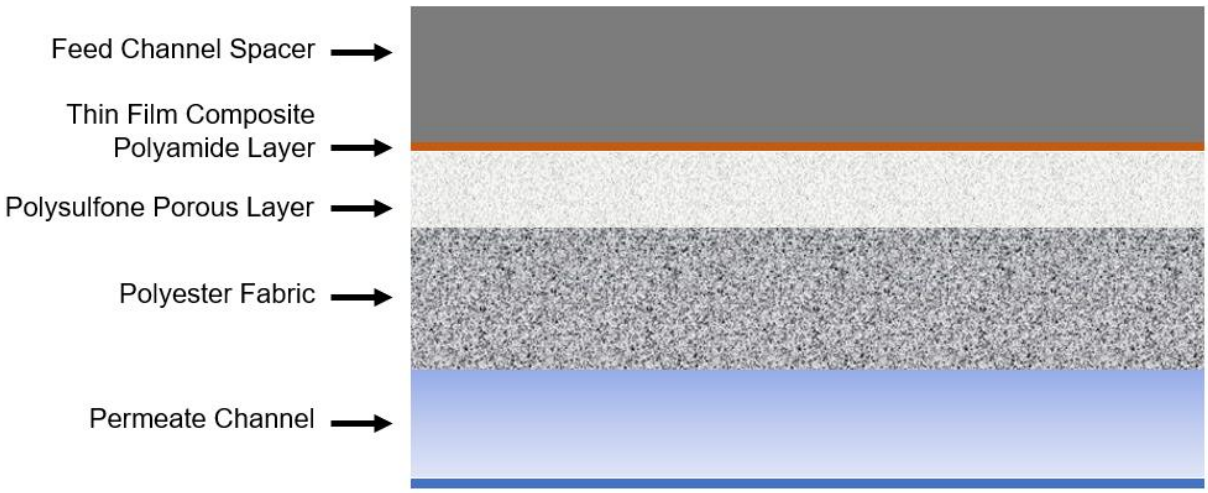

Figure 2.1 Schematic drawing of a typical RO membrane. Thin Film Composite Polyamide Layer: ~0.2um; Polysulfone Layer: ~40 um.

2.1.1. Basic concepts and definitions

RO desalination process is conducted primarily in the configuration of cross-flow filtration, as illustrated in Figure 2.2. The feed stream of flow rate F_f, pressure P_f, and concentration C_f enters the RO membrane channel, where is it separated into two streams -concentrate and permeate. The feed that passes through the membrane is the low salinity permeate of flow rate F_p, pressure P_p, and concentration C_p. The concentrate of flow rate F_c, pressure P_c, and concentration C_c, contains the solutes and particles that are rejected by the membrane.

The retentate refers to the part of the feed that does not pass through the membrane. The retentate has concentration of C_r.

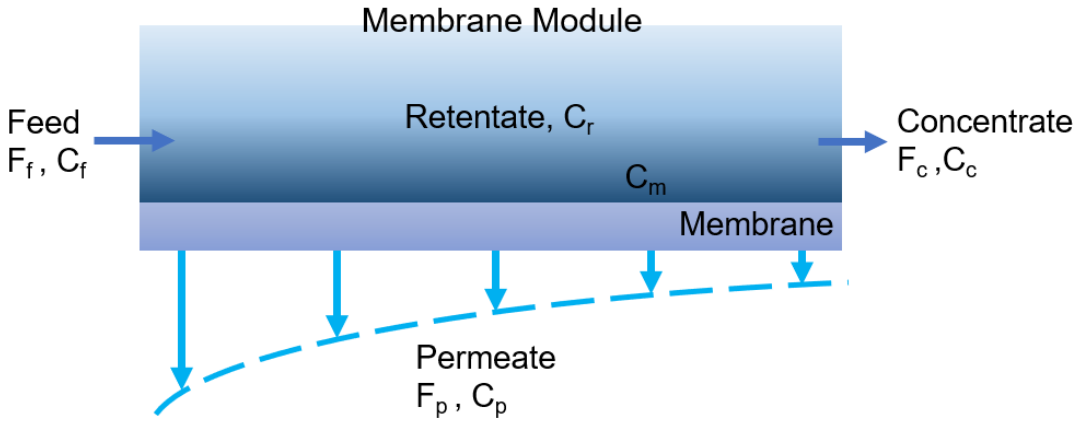

Figure 2.2. Simplified diagram of typical RO membrane module. *F* and *C* represents flow rate and concentration, respectively. The subscripts *f*, *c*, *p*, *r*, and *m* represents feed, concentrate, permeate, retentate, and membrane, respectively.

A total and salt mass balances around the RO membrane module can be written as provided below:

$$F_f = F_c + F_p \tag{1}$$

$$C_f F_f = C_c F_c + C_p F_p \tag{2}$$

in which F_f, F_c, and F_p are the flow rates of the feed, concentrate and permeate streams, respectively, and C_f, C_c, and C_p are the corresponding salt concentrations. The permeate water recovery is defined as the ratio of the permeate flow rate to the feed flow rate:

$$Y = \frac{F_p}{F_f} = \frac{F_p}{F_c + F_p} = \frac{F_f - F_c}{F_f} \tag{3}$$

and the degree by which the RO exit stream is concentrated relative to the feed is given by the concentration factor, CF:

$$CF = \frac{C_c}{C_f} \tag{4}$$

The observed membrane salt rejection is defined by:

$$R_{obs} = \frac{C_f - C_p}{C_f} = 1 - \frac{C_p}{C_f} \tag{5}$$

and the salt passage is defined as:

$$SP = 1 - R_{obs} \tag{6}$$

The intrinsic rejection, R_{intr}, is defined based on the feed-side concentration at the membrane surface, C_m, as given by:

$$R_{intr} = \frac{C_m - C_p}{C_m} = 1 - \frac{C_p}{C_m} \tag{7}$$

The permeate flux through the membrane surface is given by the classical flux expression [11]:

$$J_v = L_P\ (\Delta P - \ \sigma \Delta \pi) \tag{8}$$

where J_v is the volumetric permeate flux, L_P is the membrane permeability, ΔP is the pressure difference across the membrane, σ is the reflection coefficient, and $\Delta \pi$ is the difference in osmotic pressure across the membrane. The average applied pressure or equivalently the average transmembrane pressure in Eq. (8) is given by:

$$\Delta P = P_f - \left(\frac{P_f - P_c}{2}\right) - P_p \tag{9}$$

where P_f, P_c, and P_p are the pressures of the feed, exit concentrate stream, and permeate streams, respectively.

The osmotic pressure difference in Eq. (8) is given by:

$$\Delta \pi = \pi_m - \ \pi_p \tag{10}$$

where π_m and π_p are the osmotic pressures of the feed and permeate respectively, at the membrane surface. The osmotic pressure can be estimated from the following simple relation:

$$\pi = \phi MRT \tag{11}$$

where M is the molarity of the solution, R is the ideal gas constant, T is the temperature in Kelvin, and ϕ is the Van't Hoff Factor. The Van't Hoff Factor is determined by the number of ions in the solute and for NaCl solution takes on the value of 2.

The solute flux through the membrane, J_s, is given by the following classical expression [12]:

$$J_s = J_v \cdot C_p = L_s \, \Delta C + (1 - \sigma) \cdot J_v \cdot \bar{C} \tag{12}$$

and the concentration difference (ΔC) is give as:

$$\Delta C = C_m - C_p \tag{13}$$

where J_v is solvent molar flux, C_p is the permeate concentration, L_s is solute permeability coefficient, and $\bar{C}$ is arithmetic average of C_m and C_p.

2.1.2. Concentration polarization

In a membrane separation process, the solute that does not pass through the membrane accumulates near and at the membrane surface feed side. This solute accumulation leads to a higher solute concentration at the membrane surface relative to the bulk solution (i.e., outside the concentration boundary layer, away from the membrane surface). The above provides a concentration driving force for solute back diffusion in the direction opposite to the solute flux, as illustrated in Figure 2.3.

Solute concentration at the membrane surface can be estimated by the following simple steady-state, one-dimensional solute mass balance:

$$J_s = J_v \cdot C_p = J_v C - D \left(\frac{dC}{dx} \right) \tag{14}$$

where D is the solute diffusion coefficient in water and C is the solute concentration in the boundary layer. The concentration boundary conditions are:

$$y = 0, C = C_m \tag{15}$$

$$y = \delta, C = C_b \tag{16}$$

where C_m and C_b are the solute concentrations at the membrane surface and the bulk, respectively.

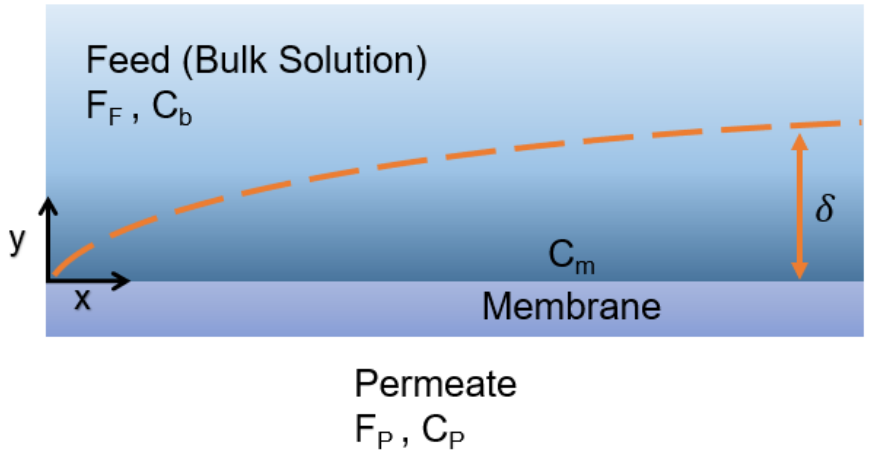

Figure 2.3. Schematic illustration of concentration profile of the solute in a RO membrane module. C_b: Bulk solution concentration; C_m: Feed-side membrane concentration; C_p: Permeate concentration; δ: Concentration boundary layer thickness.

Integration of Eq. (14) with the above boundary conditions (Eq. (15, 16)) yields the concentration polarization factor, *CP*:

$$CP = \frac{C_m - C_P}{C_b - C_P} = \exp\left(\frac{J_v \cdot \delta}{D}\right) = \exp\left(\frac{J_v}{k}\right) \tag{17}$$

where δ is the boundary layer thickness and k is the solute mass transfer coefficient. Eq. (17) can also be expressed in terms of the observed and intrinsic solute rejection as given below:

$$CP = \frac{C_m - C_P}{C_f - C_P} = \exp\left(\frac{J_v}{k}\right) = \frac{R_{intr}(1 - R_{obs})}{R_{obs}(1 - R_{intr})} \tag{18}$$

2.2. Approaches to mitigate membrane scaling

In general, the primary foulants of concern in RO membranes processes are organics, biofoluants (typically associated with algae), particulate matter and mineral scalants. Mineral scaling occurs when the concentration of sparingly soluble mineral salts exceeds their solubility limits in the RO feed channel, particularly at high recovery. Though the occurrence of mineral scaling is site-specific, three common problematic foulants are gypsum (calcium sulfate dihydrate), calcite (calcium carbonate), and barite (barium sulfate) [13]. There are different methods to prevent scaling on membrane surfaces, including feed pH adjustment and dosing of antiscalants into the RO feed.

Feed pH adjustment involves the addition of acids or bases to the RO feed. NaOH is commonly utilized to raise the feed pH and hydrochloric acid or sulfuric acid are used to lower the feed pH. pH adjustment to acidic level serves to prevent the calcite scaling, given the higher solubility of calcium carbonated at pH < 7. pH adjustment to basic level can be employed to avoid silica scaling. The solubility of gypsum and barite are not pH dependent over the pH range typically encountered in RO desalination. Therefore, antiscalants are dosed into the RO feed to suppress gypsum scaling. Antiscalants are also utilized to suppress scaling of calcite, barite, and silica. Antiscalants are typically polyelectrolytes such as polycarboxylates, polyacrylates, polyphosphonates and polyphosphates [8,14,15]. Various studies have shown that, in supersaturated solutions of sparingly soluble salts, antiscalants significant delay the crystal nucleation and subsequent growth [16]. Antiscalant actions are through one combination of the following mechanisms: threshold inhibition of nucleation, crystal surface adsorption and dispersion [17]. Antiscalants are reported to be most effective when RO operation is such that the saturation indices of the scalants of concern in the RO channel are in the following ranges: $SI_{CaCO3} \leq 60$, $SI_{SrSO4} \leq 8$, $SI_{CaSO4} \leq 2.3$, $SI_{SiO2} \leq 1$ [18,19].

2.2.1. NFF-FFR

An alternate approach to mitigating membrane surface scaling can be achieved via RO Feed flow reversal (FFR) [9]. By periodically reversing the normal feed flow (NFF) direction of the raw RO feed, mineral scale that develops at the membrane stage exit can be removed via dissolution and the membrane permeability is then recovered. When the feed water flows in the original (initial forward) direction, water flux axially decreases (Figure 2.4). Solutes accumulate on the membrane surface and when supersaturation conditions are reached, mineral scaling can occur beginning at the exit of the membrane channel. FFR is triggered when mineral scaling reaches a specific threshold. Upon FFR triggering, the feed is redirected to enter the membrane through the "exit" of the membrane module in NFF operation mode, while the previous step of stream "entrance" to the membrane module is then designated as the concentrate stream. As the entrance "exit" (scaled in the previous NFF period) is exposed to the undersaturated raw feed, mineral crystals at the membrane surface are dissolved; this eventually results in reversing permeate flux profile as shown in Figure 2.5. For effective application of FFR, it is critical that the feed is sufficiently undersaturated, as the saturation level of the feed will dictate how quickly the mineral scalant can be dissolved. The process of mineral crystallization on the membrane surface varies temporally when water feed quality and operating conditions vary. Moreover, crystal nucleation is a stochastic process which can also be impacted by RO operating conditions. Thus, a robust implementation of FFR requires by real-time membrane monitoring to enable automated FFR triggering.

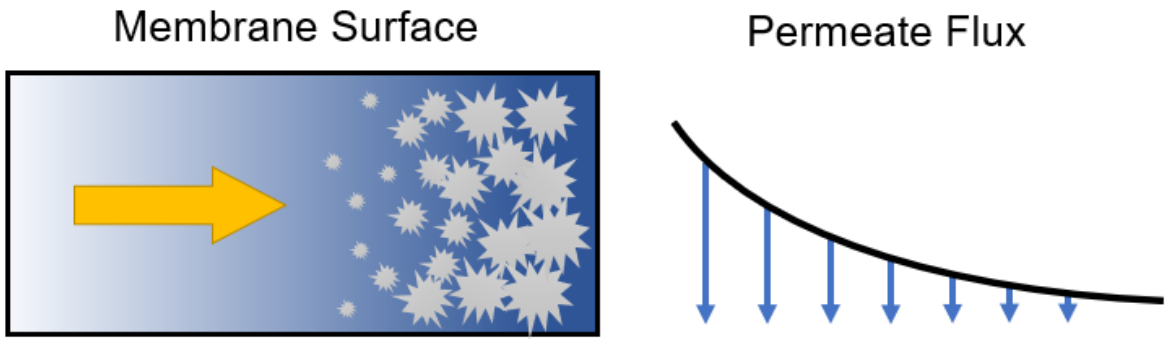

Figure 2.5. Axial permeate flux profile (right) and mineral scaling representation (left) in normal feed flow (NFF). Mineral scaling is more pronounced toward the exit of the membrane element.

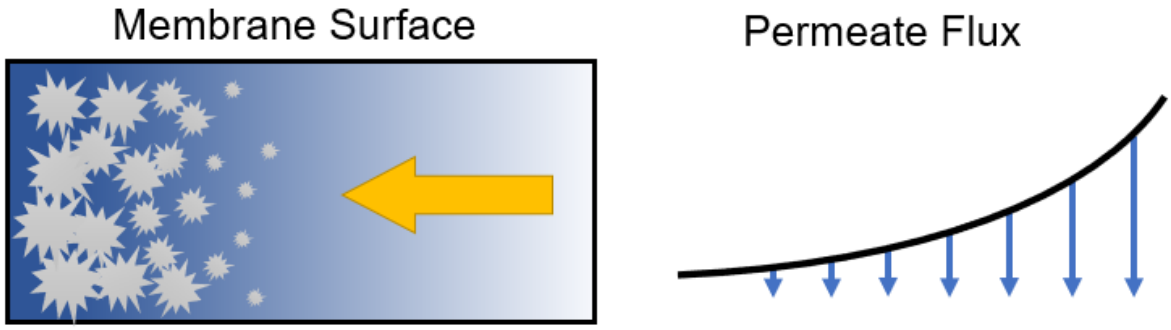

Figure 2.4. Axial permeate flux profile (right) and mineral scaling representation (left) in reversed feed flow (FFR). Previously accumulated crystals are dissolved and new accumulation begins toward the other end of the membrane channel.

In previous work [9], the concept of FFR was examined using a pilot RO unit with 6 spiral-wound RO membrane elements (6.35 cm (2.5 inches) inner diameter and 101.6 cm (40 inches) long). The first RO element to which the feed is delivered was referred to as the lead element, whereas the last element the feed passes through is referred as the tail element. The study was with a pilot RO system of 7,000 gallons/day capacity. A membrane surface monitoring system was integrated with the RO system for real-time membrane surface analysis. The study with a feed solution that was a factor of 3 above saturation with respect to gypsum, confirmed that RO operation up to 63% recovery was feasible without the use of antiscalants (Figure 2.6). NFF/FFR

tests over 15 cycles revealed that the cycle periods varied in length, presumably due to the stochastic nature of surface nucleation. It is noted that in one of the experiments in the above previously reported study [9], the RO system was run for a prolonged cycle without FFR in order to assess the efficacy of FFR. The system was operated only under normal feed flow (NFF) operation at 69% recovery with a feed gypsum saturation index of 0.44. After four hours, the fractional crystal surface coverage in the membrane monitoring cell indicated complete coverage by mineral scale. As the fractional surface coverage increased, the total and tail element permeate flow rates decreased to nearly half of the initial permeate flow rate. The above test indicated that RO operation would not be feasible without either FFR or antiscalant dosing of the RO feed.

Although FFR was demonstrated to be effective in limited tests [9,20,21], direct evidence of scale dissolution during FFR was not provided. It is noted that previous studies that utilized a membrane scale monitor in a configuration that only monitored the tail element in the NFF and FFR modes (i.e., the membrane surface monitoring system only monitored the tail element in each operational mode) [9]. Therefore, it was unclear whether the formed mineral scale was completely removed in the FFR period from the element that was the tail element in NFF. In contrast, in the present work, the objective was to capture the actual operational history of the element as it transitions from being the tail element in NFF to the lead element in FFR. Accordingly, a membrane monitoring device was utilized to monitor one end of the series of RO membranes in both the NFF and FFR modes in order to observe and analyze the complete process of crystal formation and dissolution.

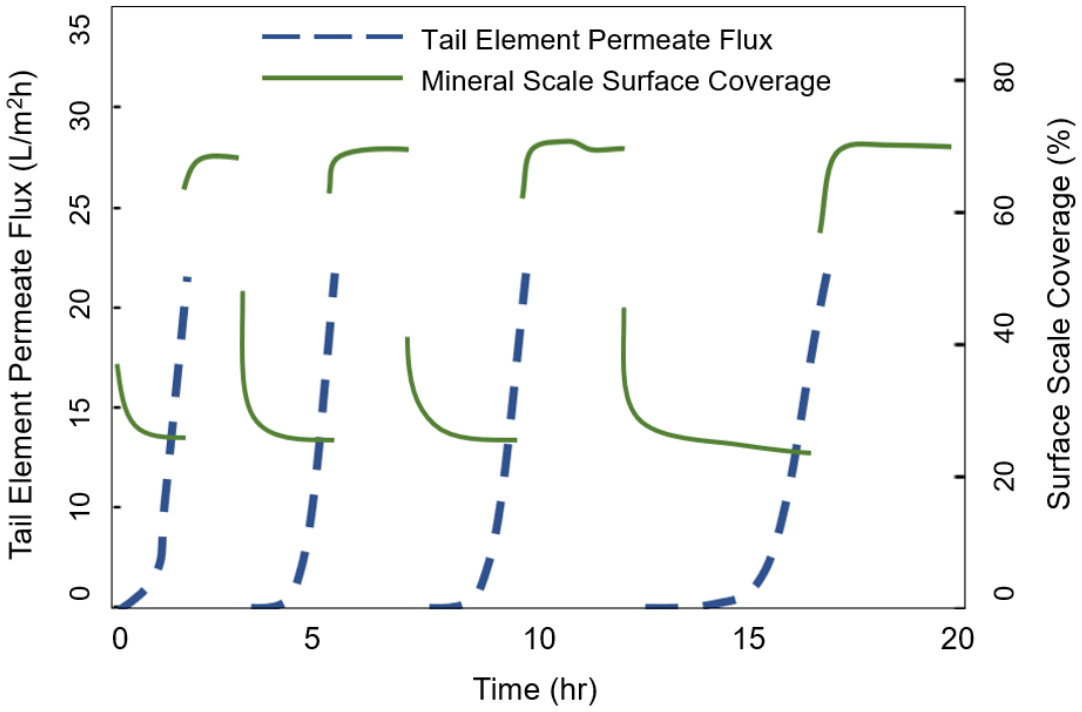

Figure 2.6. Tail element permeate flux and percent mineral scale coverage from Test 2. Figure adapted from Han, Gu. Total of 88 hours continuous operation with feed SI_{gypsum} of 0.44 and recovery of 69.1%. Feed flow rate was 0.44 m^3/hr (1.94 gpm). Figure adapted from Gu [9].

2.3. Pressure Barrier and Energy Consumption in RO Processes

The utility of RO-NF process configuration is explored with aim of reducing pressure. However, it is noted that the feed pressure affects the energy consumption in RO processes. Therefore, it is important to evaluate the energy consumption in these processes. Accordingly, in this section, analysis of the energy consumption in conventional RO and RO-NF processes are reviewed, followed by presentation of experimental data presented in Section 5.2.

2.3.1. Energy Consumption in a Conventional RO Process

In a typical RO process (single stage, single pass), shown in Figure 2.7, the feed pressure requirement is dependent on the osmotic pressure of the RO concentrate as stated below:

$$P_{RO} \geq \pi_{c,RO} \tag{19}$$

where P_{RO} is the feed pressure and $\pi_{c,RO}$ is the osmotic pressure of the RO concentrate.

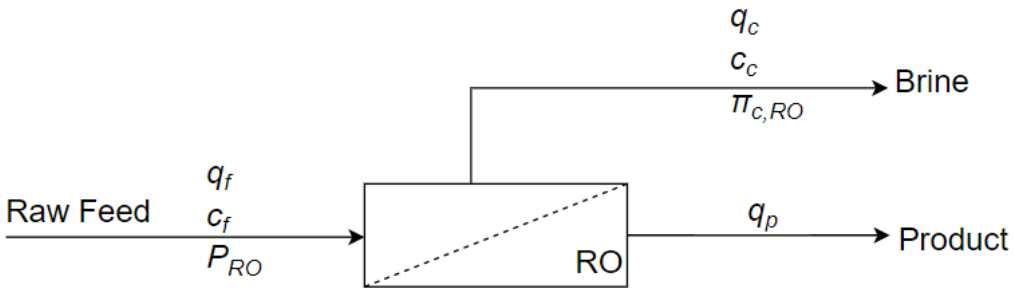

Figure 2.7. Schematic drawing of a conventional RO process. Q and C denote the flow rate and salt concentration, respectively; Subscripts: F-feed, C-Concentrate, P-Permeate.

Given that the osmotic pressure is proportional to concentration [22], the minimum pressure (imposed by the thermodynamic restriction [6], $P_{RO,min}$), for high salt rejecting membranes, is given by:

$$\frac{P_{RO,min}}{\pi_o} = \frac{c_{c,RO}}{c_{f,RO}} = \frac{1}{1 - Y_{RO}} \tag{20}$$

in which Y_{RO} is the product water recovery (i.e., $Y_{RO}=q_p/q_f$) and where $\pi_{c,RO} = \pi_o/(1 - Y_{RO})$, π_o being the raw feedwater osmotic pressure. The specific energy consumption (SEC) and normalized specific energy consumption (NSEC) of the RO process is defined by:

$$SEC = \frac{\text{Energy Consumption}}{\text{Water Productivity}} = \frac{\dot{W}_{pump}}{q_p} \tag{21}$$

$$NSEC = \frac{SEC}{\pi_o} \tag{22}$$

where the energy consumption is the energy delivered by the pump to pressurize the feed (P_f), determined as:

$$\dot{W}_{pump} = P_f \times q_f \times \eta_p \tag{23}$$

where η_p is the pump efficiency. For a single stage single pass RO process, Eq. (21, 22) can be expressed as:

$$SEC = \frac{P_f}{Y_{RO}} \tag{24}$$

$$NSEC = \frac{1}{Y_{RO}}\left(\frac{P_f}{\pi_o}\right) \tag{25}$$

and the normalized SEC (i.e., NSEC) at the limit of thermodynamic restriction (*tr*) is given by:

$$NSEC_{tr} = \frac{1}{\pi_o \cdot q_p}\left(\frac{q_f \cdot P_{min}}{\eta_p}\right) = \frac{P_{min}}{\pi_o \cdot Y_{RO} \cdot \eta_p} \tag{26}$$

where P_{min} is the minimum feed pressure. For the case of an ideal pump, the NSEC for a single stage RO can be written as:

$$(NSEC_{tr})_{RO} = \frac{1}{Y_{RO} \cdot (1 - Y_{RO})} \tag{27}$$

For RO process that is constrained by the permeate production (i.e., RO operation is not up to the thermodynamic crossflow restriction), the optimal water recovery (i.e., the recovery at the global minimum of NSEC curve) is shifted from the global minimum of 50% recovery [6]. Thus, in order to determine the SEC for a constrained operation, Eq. (27) can be modified as shown below:

$$Q_{p,norm} = \frac{Q_p}{A_m L_p \pi_o} = \frac{\Delta P - \overline{\Delta\pi}}{\pi_o} = \frac{\Delta P}{\pi_o} - \frac{\overline{\Delta\pi}}{\pi_o} \tag{28}$$

where Q_p is the volumetric permeate flux, A_m is the active membrane area, L_P is the membrane hydraulic permeability, π_o is the feed osmotic pressure, ΔP is the pressure difference across the membrane, $\Delta\pi$ is the average osmotic pressure difference between the retentate and permeate streams along the membrane module, and $Q_{p,norm}$ is the normalized permeate flow. Accordingly,

the NSEC for the permeate flow rate constrained RO processes, $(NSEC_{tr})_{RO,Perm}$, can be expressed as:

$$(NSEC_{tr})_{RO,Perm} = \frac{Q_{p,norm}}{Y_{RO}} + \frac{\ln\left(\frac{1}{1-Y_{RO}}\right)}{Y_{RO}} \tag{29}$$

2.3.2. Energy Consumption in RO-NF Process

Desalination using RO-NF configuration involves having a conventional RO process followed by NF process (Figure 2.8). In the RO-NF process, product water is produced primarily in the RO stage, while the function of the NF stage is to further concentrate the RO concentrate. The recycled NF permeate is then delivered to the RO feed, in order to lower the osmotic pressure of the RO feed relative to the raw feed.

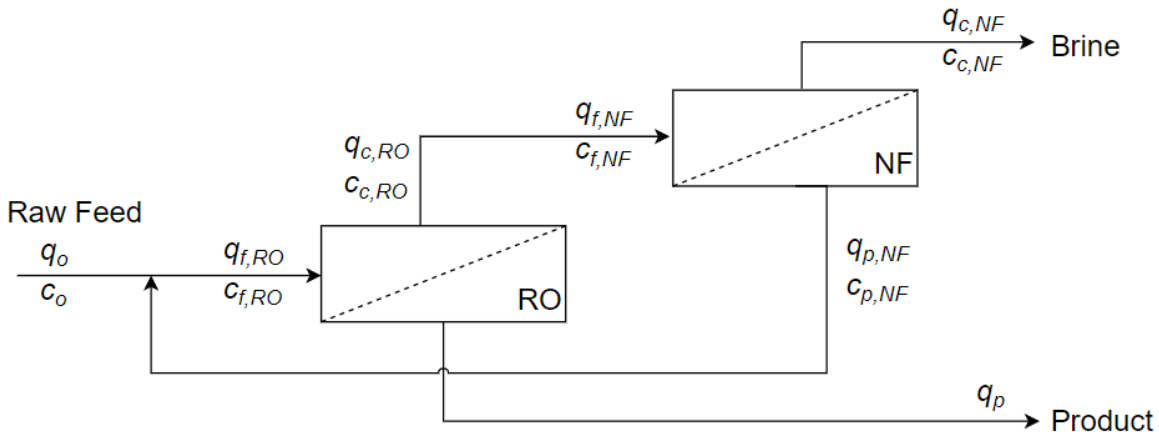

Figure 2.8. Schematic illustration of the RO-NF process. Q and C denote the flow rate and salt concentration, respectively.; Subscripts: F-feed, C-Concentrate, P-Permeate.

The recovery in the NF stage (Y_{NF}) is defined as:

$$Y_{NF} = \frac{q_{p,NF}}{q_{f,NF}} \tag{30}$$

where $q_{p,NF}$ and $q_{f,NF}$ are the NF permeate and feed flow rates, respectively. The overall system recovery (Y_T) can be derived (Appendix B.1) to yield:

$$Y_T = \frac{Y_{RO}}{1 - Y_{NF} \cdot (1 - Y_{RO})} \tag{31}$$

in which Y_{RO} (=$q_p/q_{f,RO}$) and Y_{NF} (=$q_{p,NF}/q_{f,NF}$) are the recovery levels of the RO and NF stages, respectively. Because in this study, Y_{RO} is defined as $q_p/q_{f,RO}$, where $q_{f,RO}$ is the sum of raw feed (q_o) and recycled NF permeate ($q_{p,NF}$), the specific energy consumption (SEC) and normalized specific energy consumption (NSEC) of the RO-NF process are the same with Eq. (24) and Eq. (25), respectively.

Intrinsic salt rejection of the NF membrane, $R_{i,NF}$, is expressed as [11] :

$$R_{i,NF} = 1 - \frac{1 - \sigma_x}{1 - \sigma_x \cdot F} = 1 - \frac{C_{P,NF}}{C_{m,NF}} \tag{32}$$

where σ_x is the local membrane solute reflection coefficient, $C_{p,NF}$ is the permeate salt concentration, and $C_{m,NF}$ is the retentate salt concentration near the membrane (as illustrated in 2.1.2), and where F is defined by:

$$F = exp\left(-\frac{(1 - \sigma_x)}{k_{s,x}} \cdot J_x\right) \tag{33}$$

where $k_{s,x}$ is the local solute membrane permeability coefficient and J_x is the local solvent flux. Since k_s is large for NF membranes, F can be assumed to be negligible (i.e., $F \approx 0$) and thus Eq. (33) can be reduced to $R_{i,NF} \approx \sigma_x$. Accordingly, the relationship between the intrinsic and observed salt rejection can be derived from a one-dimensional differential mass balance along the length of the NF retentate channel, yielding:

$$R_{i,NF} = 1 - \frac{ln\big(1 - (1 - R_{obs,NF}) \cdot Y_{NF}\big)}{ln(1 - Y_{NF})} \tag{34}$$

The minimum feed pressure can be derived based on flow and salt balances on the first-stage

RO (Appendix B.2) leading to:

$$\frac{(P_{RO,min})_{RO-NF}}{\pi_o} = \frac{1 - Y_{NF}(1 - Y_{RO})}{(1 - (1 - R_{NF}) \cdot Y_{NF}) \cdot (1 - Y_{RO})} \tag{35}$$

and required feed pressure for the NF elements is given by:

$$P_{NF} \geq \pi_{c,NF} \tag{36}$$

where P_{NF} and $\pi_{c,NF}$ are NF feed pressure and osmotic pressure of the NF concentrate, respectively. At the thermodynamic restriction limit, the minimum required NF feed pressure ($P_{NF,min}$) is:

$$\frac{P_{NF,min}}{\pi_{f,NF}} = \sigma_{NF} \cdot R_{NF} \cdot \frac{C_{c,NF}}{C_{f,NF}} \tag{37}$$

where $\pi_{f,NF}$, σ_{NF} are NF feed osmotic pressure, NF solute reflection coefficient and $C_{c,NF}$, $C_{f,NF}$ are the concentrate and feed concentrations, respectively. Combining Eq. (37) and Eq. (31) yields:

$$\frac{(P_{NF,min})_{RO-NF}}{\pi_o} = \frac{\sigma_{NF} \cdot R_{NF}}{1 - Y_T} \tag{38}$$

where π_o is the osmotic pressure of raw feed. Upon combining Eq. (38) and Eq. (27), the normalized SEC at thermodynamic restriction limit is given by:

$$(NSEC_{tr})_{RO-NF} = \begin{cases} \frac{1}{Y_{RO}} \cdot \frac{P_{RO,min}}{\pi_o} & \text{if } P_{RO,min} \geq P_{NF,min} \\ \frac{1}{Y_{RO}} \cdot \frac{P_{NF,min}}{\pi_o} & \text{if } P_{RO,min} < P_{NF,min} \end{cases} \tag{39}$$

The NSEC curves at the thermodynamic restrictions for the RO and RO-NF processes are shown in Figure 2.9. The analysis indicates that the NSEC is lower for the RO-NF configuration once RO recovery exceeds about 20%.

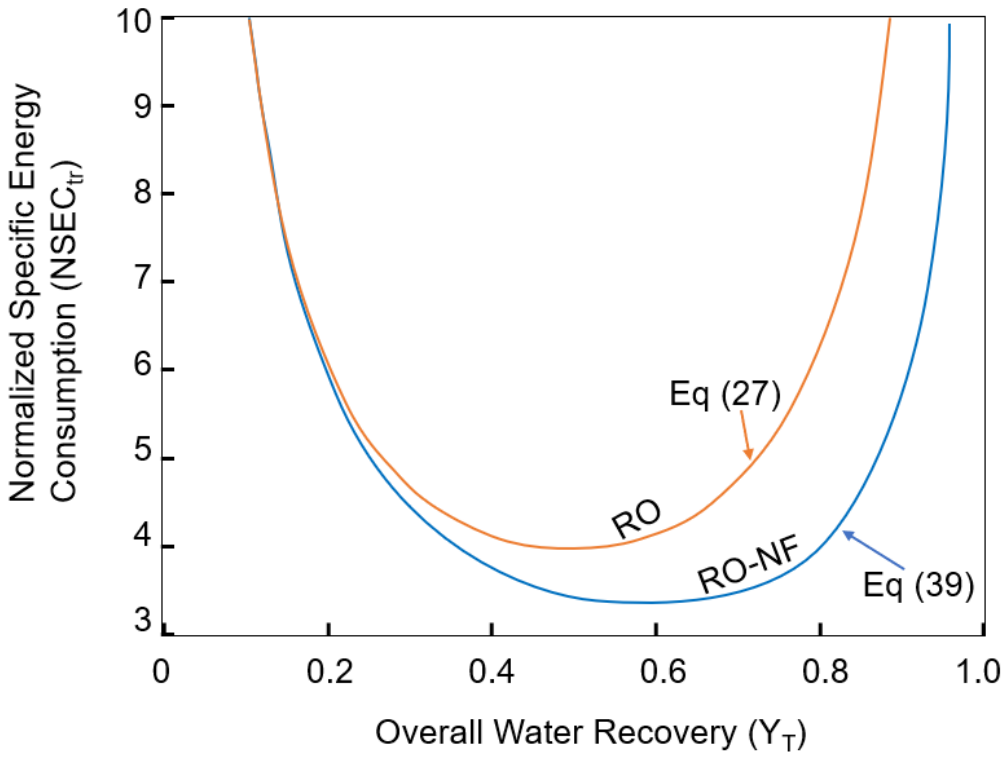

Figure 2.9. Normalized specific energy consumption (NSEC) for RO and RO-NF process configurations at pressure-optimal conditions (i.e., with respect to NF intrinsic salt rejection).

.

3. Description of System

3.1. Description of the Mini, Mobile, Modular (M3) RO System

3.1.1. Design concepts of M3 System

A mini, mobile modular (M3) RO system was constructed consisting of a pump module and a separate membrane module. The pump module contained a booster pump, high-pressure pump, heat exchanger, and various sensors. The membrane module included six pressure vessels, 3-way valves, and various sensors. The pump module pressurizes the raw feed in the tank and the membrane module separates the feed into retentate and permeate streams.

3.1.2. Pump Module

In the pump module, raw feed water is first pressurized by a booster pump (JM3460, Baldor), having a power capacity of 0.37 kW (0.5 hp). The feed flows through a plate heat exchanger (BrazePak BP 410-30, Xylem, California) that can withstand a pressure up to 3,000 kPa (435 psi). The heat exchanger serves to maintain the RO feed stream temperature. The feed is then passed through a 0.2 micron polysulfone plastic filter (43765K34, McMaster-Carr, California) to remove mineral scale particles present in the recycled RO retentate.

The flow rate, conductivity, and pressure were measured before the feed delivery to the high pressure feed pump. The flow rate was measured by flow sensors (3-2537-1C-P0, GF Signet, California) having a measurement range of 0.11-11.34 m^3/hr (0.5-50 gpm) and maximum operating pressure of 1,241 kPa (180 psi) and temperature up to 65°C (149 °F). Due to the pressure limit, the flow sensor was installed after the booster pump and before the main feed pump. Feed conductivity was measured with GF Signet's 3-2850-52-42V conductivity meter, having an operational range of 100 uS/cm to 200,000 uS/cm. This range was sufficient for measuring feed

with TDS up to about 108,000 ppm. A pressure transducer (A-10, 0-25 psi, WIKA, Georgia) was installed before the main pump having a pressure measurement range of 0-172 kPa (0-25 psi), and a pressure transducer (A-10, 10-1000 psi, WIKA, Georgia) was installed after the RO high pressure feed pump.

A stainless steel (316SS) RO feed pump rated for 480V (5 frame plunger pump 351, CAT Pumps, Minnesota) was capable of pressurizing the feed from 68.9 to 103.42 bar (10 to 1500 psi) at a flow rate capacity of $3.15 \cdot 10^{-4}$ m^3/sec (5.0 gpm). The power supply for the pump variable frequency drive (IP66, ABB, Wisconsin) was used to adjust the pump output flow rate and pressure. The pressurized feed was delivered to the membrane module via a high-pressure stainless steel braided hose rated for a pressure up to 13,790 kPa (2,000 psi). The process flow diagram of the pump module is shown in Figure 3.1 with the various components listed in Table 3.1.

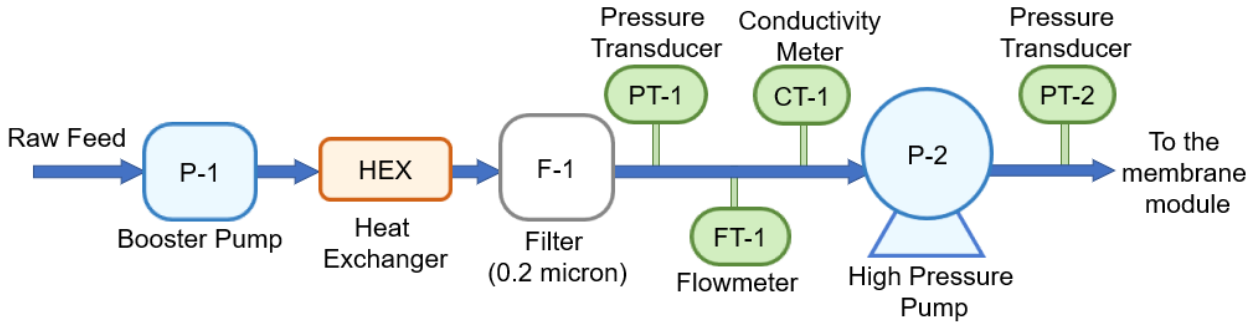

Figure 3.1. Process flow diagram of the M3 pump module.

Table 3.1. The list of parts used in the pump module.

Part Label	Part	Model Number	Manufacturer
P-1	Booster pump	JM3460	Baldor
HEX	Heat exchanger	BrazePak BP410030	Xylem
F-1	Filter	43765K34	McMaster-Carr
FT-1	Flow meter	3-2537-1C-P0	GF Signet
CT-1	Conductivity meter	3-2850-52-42V	GF Signet
PT-1	Pressure transducer	A-10 (0-25 PSI)	WIKA
P-2	High pressure pump	5 frame plunger pump 351	CAT Pumps
PT-2	Pressure transducer	A-10 (0-1000 PSI)	WIKA

3.1.3. Membrane Module

The membrane module receives pretreated, pressurized feed water. In the membrane module, six pressure vessels (FRP PV-2540SW, Hydrocomponents & Technologies, California) are installed in series. The feed water pressure in these pressure vessels is controlled with an actuated 2-way valve (MCJ-050AB, Hanbay, Virginia) placed at the retentate stream (V-1). The feed pressure in the first and last pressure vessel (PV-1 and PV-6, respectively) were measured with a pressure transducer (A-10, WIKA, Georgia) with range of 689-6,890 kPa (100-1,000 psi).

The permeate from the elements in the first (PV-1) and last (PV-6) pressure vessel were measured via a flowmeter (101 Liquid Flo-Sen, McMillan, Texas) with a measurement range of 0.01-0.12 m^3/hr (0.03-0.53 gpm). The permeate streams from all pressure vessels were combined into single stream. Subsequently, concentration, temperature, and flow rates of the combined permeate were measured. Since the permeate stream was of low salinity, the permeate stream conductivity was measured with a conductivity meter (3-2850-52-41V, GF Signet, California) that had a range of 0-10,000 uS/cm. The flow rates of both the permeate and retentate streams were

monitored with flow sensors (3-2537-1C-P0, GF Signet, California) that had a measurement range of 0.11-11.36 m^3/hr (0.5-50 gpm). The pressure of both the permeate and retentate streams were measured with a pressure transducer (A-10, WIKA, Georgia) suitable for the pressure range of 0-172 kPa (0-25 psi). Figure 3.2 provides the process flow diagram of the membrane module. A list of the membrane module component is provided in Table 3.2.

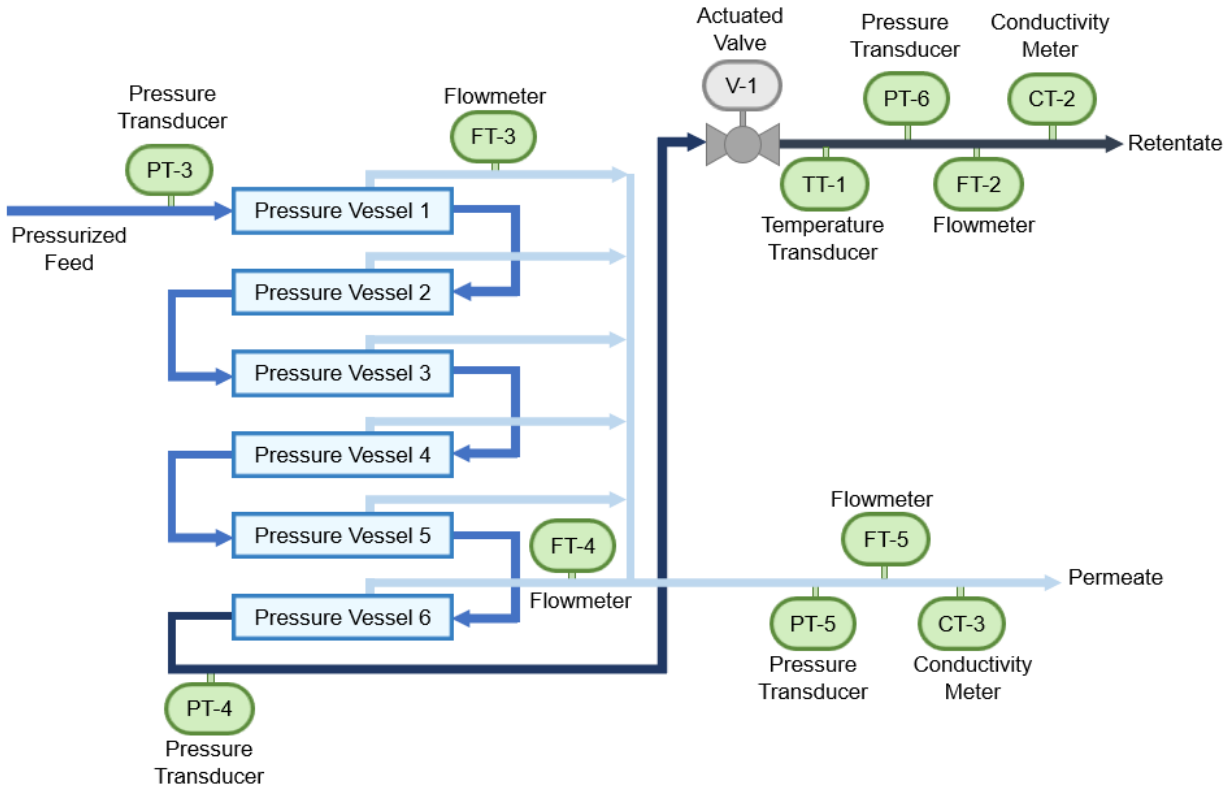

Figure 3.2. Process flow diagram of the M3 membrane module.

Table 3.2. The list of parts used in the membrane module.

Part Label	Part	Model Number	Manufacturer
PV1 – PV6	Pressure Vessels	FRP PV-2540SW	Hydrocomponents & Technologies
PT-3	Pressure transducer	A-10 (0-1000 PSI)	WIKA
PT-4	Pressure transducer	A-10 (0-1000 PSI)	WIKA
PT-5	Pressure transducer	A-10 (0-25 PSI)	WIKA
PT-6	Pressure transducer	A-10 (0-25 PSI)	WIKA
FT-2	Flow sensor	3-2537-6C-P0	GF Signet
FT-3	Flow sensor	101 Liquid Flo-Sen	McMillan
FT-4	Flow sensor	101 Liquid Flo-Sen	McMillan
FT-5	Flow sensor	3-2537-6C-P0	GF Signet
TT-1	Temperature sensor	3-2350-3	Harrington
CT-2	Conductivity meter	3-2850-52-42V	GF Signet
CT-3	Conductivity meter	3-2850-52-41V	GF Signet
V-1	Actuated 2-way valve	MCJ-050AB	Hanbay

3.1.3.1. RO system operation in mode of Feed Flow Reversal

In order to enable the operation in the mode of feed flow reversal (FFR), two 3-way valves (73E22-12EWS-D31, KZValve, Nebraska) were installed before and after the series of six membrane elements. In the normal feed flow (NFF) operational mode, the feed flows from pressure vessel 1 to pressure vessel 6. In this mode, PT-3 provided the pressure of the feed entering pressure vessel 1, whereas PT-4 provided the pressure of the concentrate exiting pressure vessel 6. The permeate flow rate from the lead element (RO membrane in pressure vessel 1) was measured by FT-3, and the permeate flow rate from the tail element (RO membrane in the pressure vessel 6) was measured by FT-4. The process flow diagram of NFF operational mode is shown in Figure 3.3.

When switching the flow direction, two three-way valves (V-2 and V-3) were manipulated via control software to simultaneously change their positions. In the FFR mode, the pressurized feed from the pump module is fed to pressure vessel 6 and exits through pressure vessel 1. PT-4 and PT-3 measures the pressure of the feed and that of the retentate, respectively. FT-4 measures the permeate flow rate from the lead element (pressure vessel 6), whereas FT-3 measures the permeate flow rate from the tail element (pressure vessel 1). The process flow diagram for the FFR operational mode is shown in Figure 3.4.

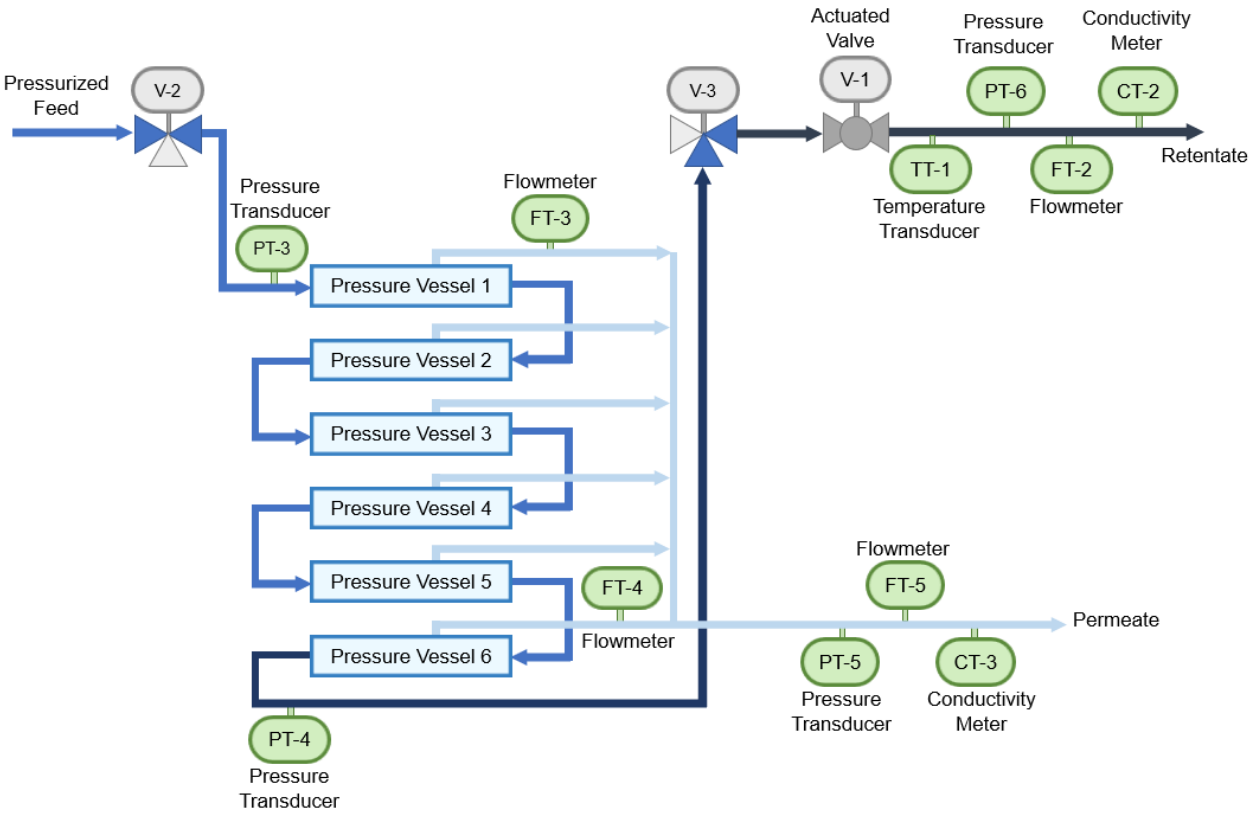

Figure 3.3. Process diagram of the membrane module when the feed flows in the normal direction (Normal Feed Flow, NFF) from pressure vessel 1 to pressure vessel 6. PT-3 monitors the feed pressure in this operational mode, whereas PT-4 monitors the concentrate pressure.

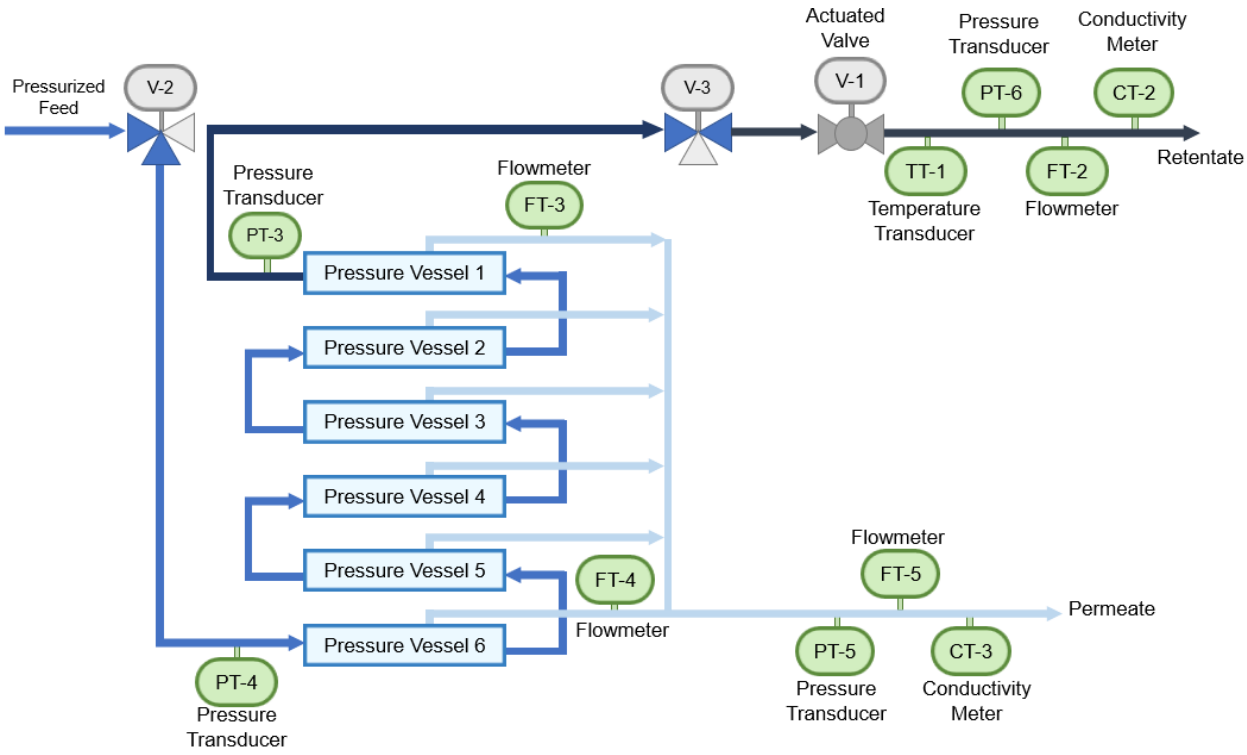

Figure 3.4. Process diagram of the membrane module when the feed flows in the reverse direction (Feed Flow Reversal, FFR) from pressure vessel 6 to pressure vessel 1. Two three-way valves, Valve 2 and Valve 3, are manipulated in order to switch the direction of feed flow. In FFR mode, PT-4 measures the feed pressure and PT-3 measures the concentrate pressure.

3.1.3.2. RO-NF Configuration

M3 was modified for the RO-NF experiments such that the NF stream was recycled and combined with the feed before it was delivered to the main pump. A sample port (V-4) was added for conductivity measurement of the recycle stream (i.e., NF permeate stream). The pressurized feed first flowed through the RO membranes and then through the NF membranes. The permeate flow rate from each NF membrane was measured with FT-3 and FT-4. The process flow diagram of M3 in RO-NF configuration is shown in Figure 3.5.

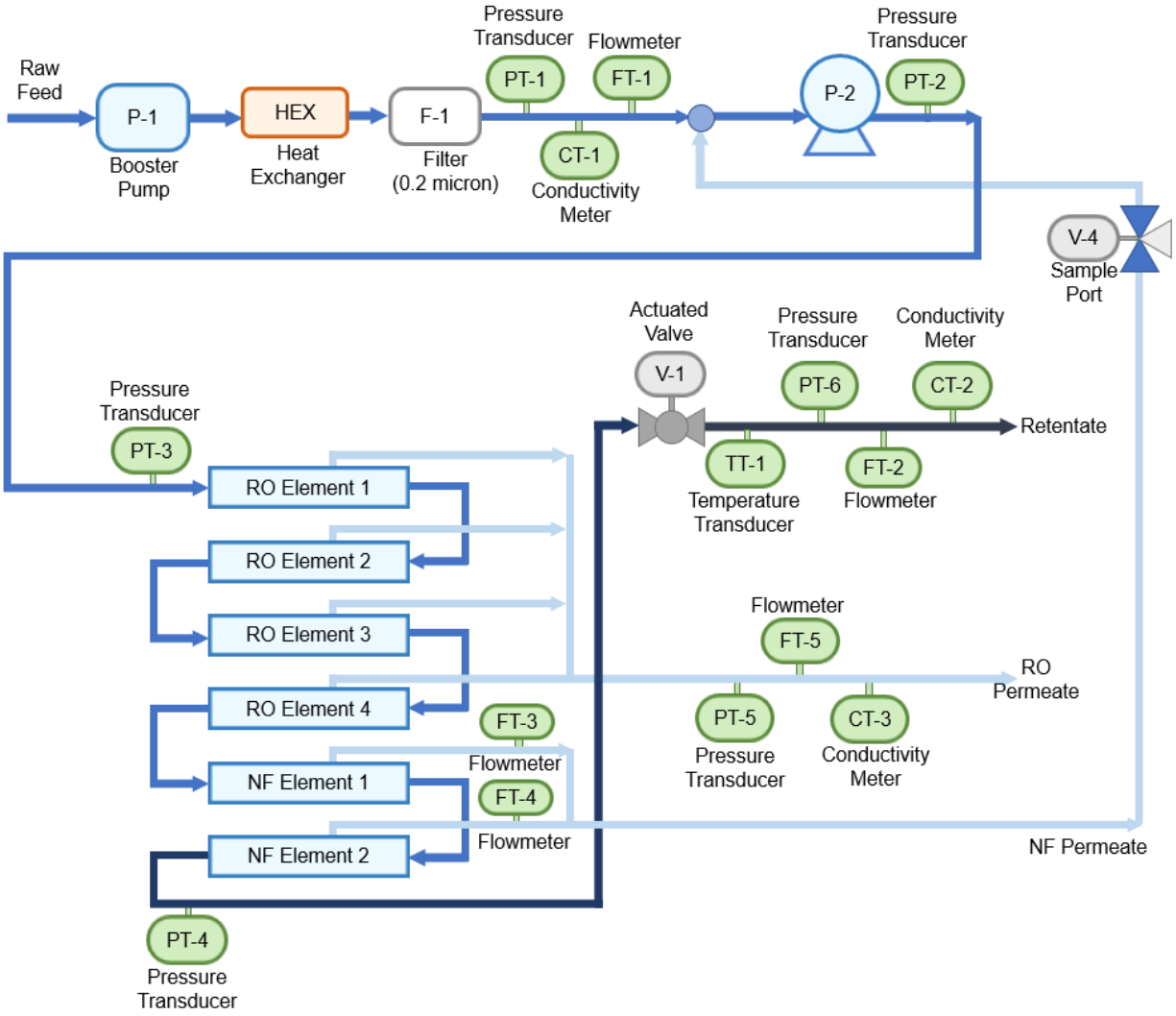

Figure 3.5. Process flow diagram of M3 in RO-NF configuration.

3.2. Membrane Monitoring Device (MMD)

A membrane monitoring device (MMD) was utilized that enabled real time-surface image analysis of membrane coupon installed in a plate-and frame RO system. MMD is capable of mimicking the condition of spiral-wound RO element. With adjustment of the feed flow rate (hence the crossflow velocity), the CP can be matched with that of the spiral-wound RO element. The schematic illustration of the membrane monitoring device is shown in Figure 3.6.

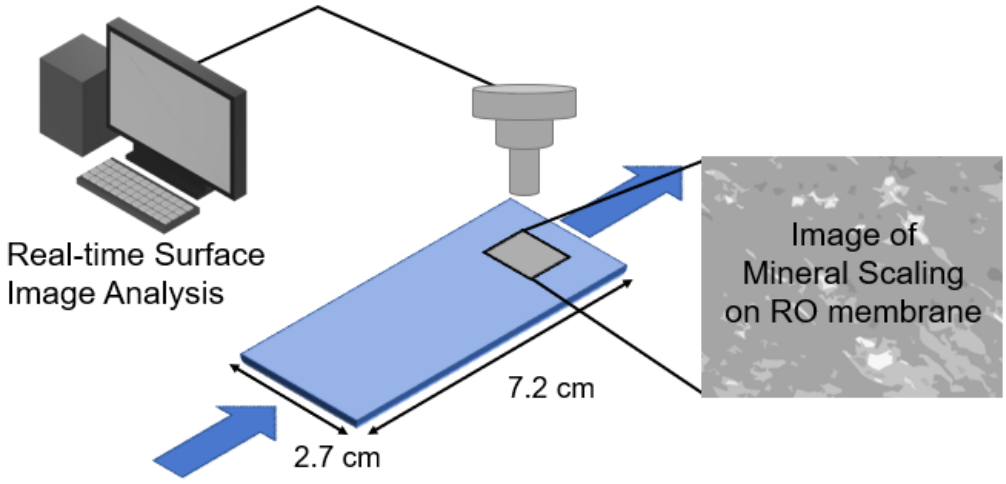

Figure 3.6. The schematic illustration of membrane monitoring device (MMD).

3.3. Data Acquisition and Control

The M3 system is controlled by a NI LabVIEW (National Instrument, Texas) program developed for the system. The feed flow rate was controlled by setting the VFD to adjust the pump speed. The pressure was controlled by adjusting the position of valve in the retentate stream (V-1). Sensors were connected to data acquisition system (CRIO, National Instruments, Texas) by which the obtained data were saved in real time.

4. Experimental

4.1. NFF/FFR

4.1.1. RO System for NFF/FFR Operation

Feed flow reversal (FFR) experiments were conducted using the RO system configuration with six spiral-wound RO elements (CSM RE 2540-BE brackish water RO element in series) housed in six pressure vessels. Each element had diameter of 6.35 cm (2.5 inches) and length of 101.6 cm (40 inches); the properties of the membrane are provided in the Table 4.1. Prior to compaction, the RO system was flushed with DI water for 24 hours. Subsequently, membrane compaction (Appendix E.3) was carried out by operating the RO system at 1,034 kPa (150 psi) feed pressure and feed flow rate of 0.34 m^3/hr (1.5 gpm) for 24 hours with 2,000 ppm of NaCl solution (Fisher Scientific, Massachusetts).

Table 4.1. The membrane module configuration and membrane properties.

Pressure Vessels	6
Element per Vessel	1
Total Elements	6
Membrane	CSM RE 2540-BE
Supplier	CSM
Membrane Type	Polyamide Thin-Film Composite
Reported Salt Rejection (NaCl)	99.8%
Permeability	$9.37 \cdot 10^{-12}$ m/s·Pa (0.137 gfd/psi)
Maximum Operating Temperature	45 °C
Maximum Operating Pressure	4137 kPa (600 psi)
Maximum Feed Flow Rate	1.36 m^3/min (6 gpm)
Minimum Feed Flow Rate	0.23 m^3/min (1 gpm)

Maximum SDI	5

4.1.2. Model Solution with system setup for NFF/FFR Study

Model feed solutions were prepared using laboratory grade anhydrous sodium sulfate and calcium chloride dihydrate (ACS grade, Fisher Scientific, Massachusetts). The concentration of the model feed solutions mimicked the composition of groundwater in San Joaquin Valley [3] (Table 4.2), for which the saturation index of gypsum (SI_g) was below unity. The solution in the feed tank was mixed using a portable mixer (NEP: A-1.0, Neptune Mixer Company, Pennsylvania). The feed solution pH was adjusted with the addition of 5 mmol NaOH solution to maintain the solution at neutral pH.

Table 4.2. The model solution composition and specification for FFR experiment. The solution mimics the composition of groundwater in San Joaquin Valley [3].

Analytes	Concentration	Unit
Na^+	20	mM
Ca^{2+}	10	mM
SO_4^{2-}	10	mM
Cl^-	20	mM
TDS	2024	mg/L
SI_{gypsum} (at 25 °C)	0.51	
pH	7.04	
Osmotic pressure	0.679	bar (9.85 psi)

4.1.3. Experimental Setup

The MMD (Section 3.2) was integrated into the RO system for real-time monitoring of mineral scaling. MMD was installed as shown in Figure 4.1 after the tail element for operational configuration in the mode of normal feed flow (NFF) mode. In feed flow reversal (FFR) mode, MMD monitoring transitioned to monitoring at the entrance of the lead element, as shown in Figures 4.1 and 4.2. Therefore, MMD was exposed to the same operational history of the same

zone in the monitored element which transitioned periodically from being the lead to become the tale zone in the RO system. When the RO system was operated in the NFF mode, the RO feed flow was from membrane 1 to membrane 6. In this operating mode the observed exit area of membrane 6 and MMD membrane surface were exposed to the exit concentrate stream. The process flow diagram of M3-2 and MMD during NFF is shown in Figure 4.1.

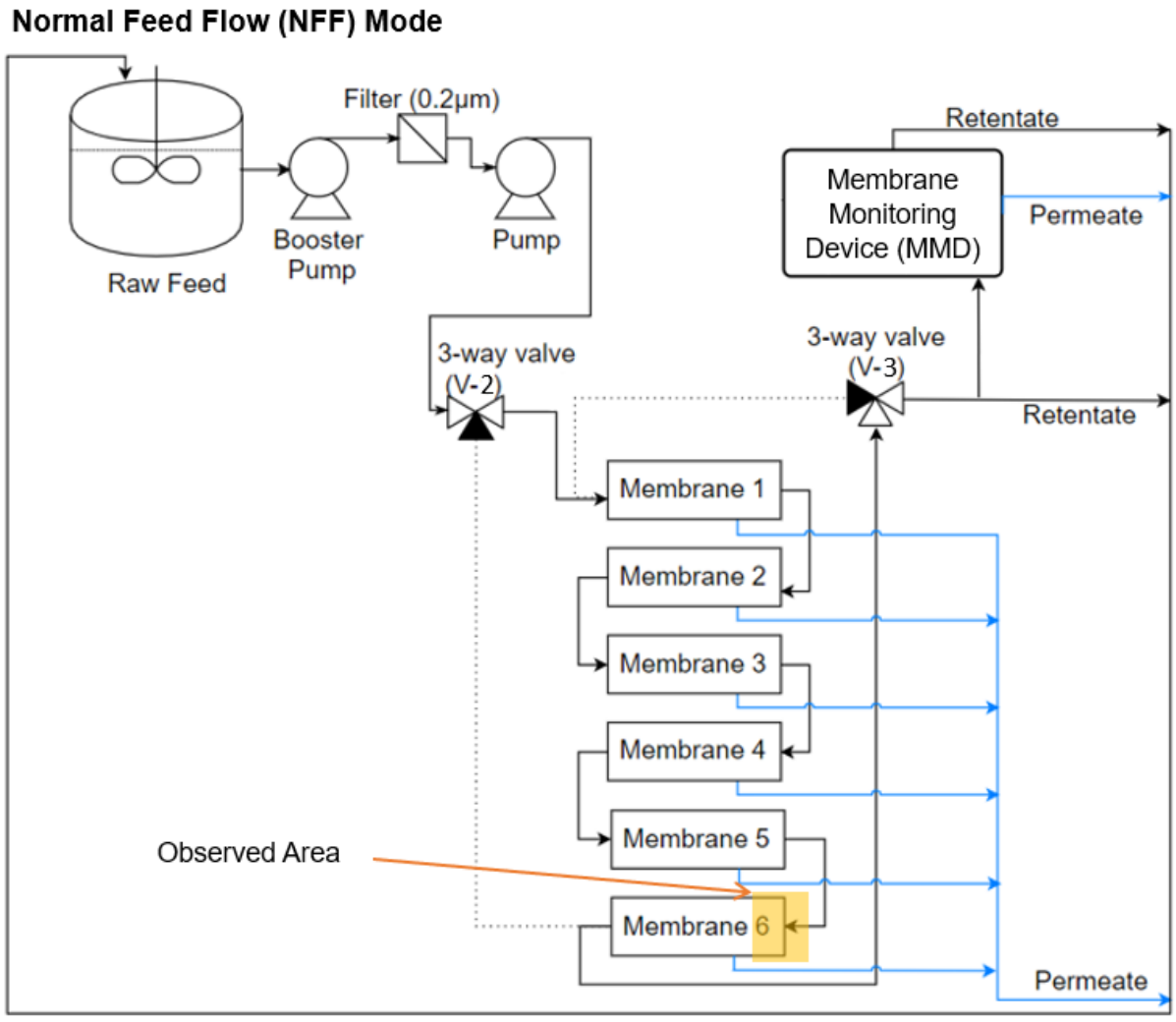

Figure 4.1. Process flow diagram of M3-2 and MMD during normal feed flow (NFF) mode.

Upon switching the operation to FFR mode, the RO feed flow direction was from membrane 6 to membrane 1. During FFR, the observed membrane and MMD membrane surface were exposed to the undersaturated feed solution. The process flow diagram for FFR is shown in Figure 4.2.

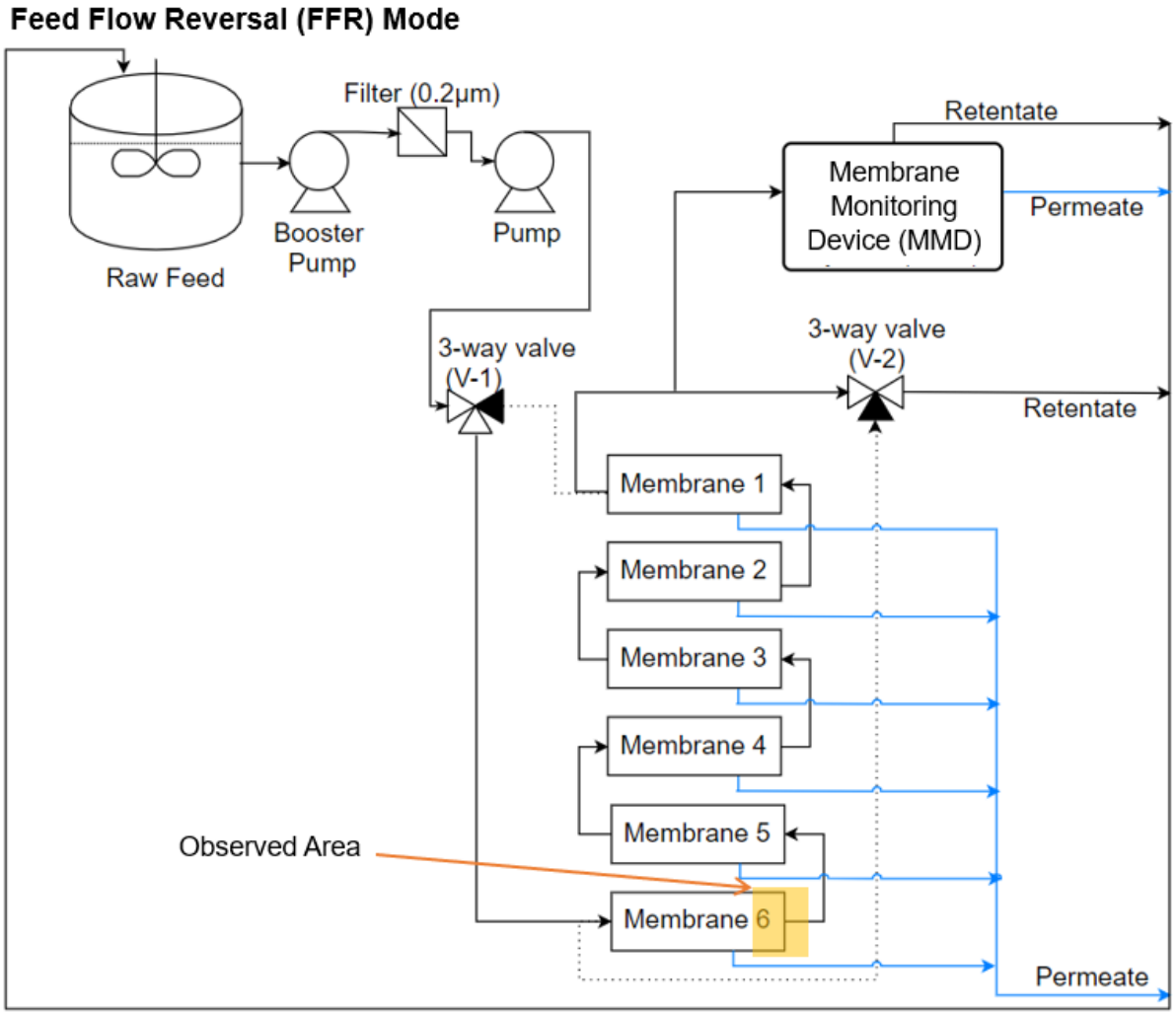

Figure 4.2. Process flow diagram of M3-2 and MMD during feed flow reversal (FFR) mode.

4.1.4. NFF/FFR Experiments

The FFR operation is most effective when the scalant saturation index (SI), gypsum (SI_g) in the present work, of feed is below unity and where SI_g of retentate is above 1. This condition was set for RO system operation at recovery of 65%, at which the retentate SI_g was 1.64 and the feed solution SI_g was 0.52. The value of SI_g was determined using a stream analysis program (OLI Studio Version 9.5, OLI Systems, New Jersey[23]).

It is critical to operate the RO system within the membrane manufacturer's specifications. Accordingly, the membrane manufacturer design software (CSMPRO v5.0, Toray Advanced Materials, Korea) was utilized to determine the appropriate operating feed flow rate and pressure ranges for the feed solution given in Table 4.2. The feed flow rate was set at 8637.6 cm^3/min (1.9 gpm), and the operating pressure was in the range of 1,407 to 1,448 kPa (204 to 210 psi). At the above flow rate and pressure, SI_g at the membrane surface for element six (Figure 4.1) was 1.85 for NFF operation and 0.53 for FFR operation.

MMD was integrated with the RO system (Figures 4.1 and 4.2). In both the NFF and FFR modes, the crossflow velocity in MMD was adjusted via a control valve to match the conditions in MMD with that in element six. However, concentration polarization (CP) and SI_g were slightly higher in MMD than in the monitored element since a channel spacer was not utilized in MMD. The channel spacer promotes mixing in the membrane channel which lowers CP, for a given crossflow and flux, relative to a channel without a spacer. It is noted that the slightly higher CP in MMD enabled early detection of scaling potential. CP in MMD was estimated using the Graetz-Lévêque equation (Appendix B.3). When the feed to the MMD had SI_g value of 1.64, the SI_g at the MMD membrane surface was 2.05 relative to 1.85 at the surface of the monitored element. The feed pressure, CP, and SI_g of the monitored element and MMD are shown in Table 4.3.

In the beginning of the experiment, the RO system was first operated in NFF mode. In NFF mode the sixth element was the tail element with a recorded operating pressure of 1,303 kPa (189 psi). In MMD, the pressure was somewhat lower 1,282 kPa (186 psi) due to a minor pressure loss associated with pipe fittings.

FFR was triggered when gypsum crystal surface coverage in the monitored MMD reached 6%. When the RO system was operated in FFR mode, the sixth element became the lead element and the pressure in the sixth element was 1,427 kPa (207 psi). The RO system was operated in FFR mode for the same duration as in NFF. Subsequently, the operational mode was switched back to NFF.

Table 4.3. Crossflow velocity, feed pressure, CP, and SI_g at the membrane surface of the monitored element (membrane 6) and MMD during normal feed flow operation (NFF) and feed flow reversal operation (FFR).

Normal Feed Flow (NFF)	**Crossflow Velocity (cm/s)**	**Feed Pressure (kPa)**	**CP**	**$SI_{g,\ surface}$**
Membrane 6	4.3	1303 (189 psi)	1.13	1.85
Membrane Monitoring Device	20	1282 (186 psi)	1.23	2.05

Feed Flow Reversal (FFR)	**Crossflow Velocity (cm/s)**	**Feed Pressure (kPa)**	**CP**	**$SI_{g,\ surface}$**
Membrane 6	12.4	1427 (207 psi)	1.02	0.53
Membrane Monitoring Device	36.2	1413 (205 psi)	1.21	0.60

4.2. RO and RO-NF

4.2.1. RO System Utilizing Different Configuration

RO-NF experiments were carried out in two configurations in order to compare the required applied pressure and specific energy consumption (SEC) of RO-NF with that of a conventional single-stage RO system configuration. For the conventional single-stage RO configuration, five RO elements were used. For the hybrid RO-NF system, four RO elements were used (in series) followed by two installed NF elements. Also, the recycle stream was added to deliver the NF permeate to the RO feed stream. The RO system had six pressure vessels. Therefore two NF elements were used in order to provide sufficient NF permeate flow rate. The membrane elements used for each configuration are listed in Table 4.4, and the process flow diagrams for the RO and RO-NF configurations are shown in Figures 4.3 and 4.4, respectively.

Table 4.4. The membrane module configuration and membrane properties of RO configuration and RO-NF configuration.

	RO configuration	RO-NF configuration
Number of RO Elements	5	4
Number of NF Elements	0	2
Element Length	101.6 cm (40 inches)	RO: 101.6 cm (40 inches) NF: 101.6 cm (40 inches)
Element Diameter	6.35 cm (2.5 inches)	RO: 6.35 cm (2.5 inches) NF: 6.35 cm (2.5 inches)
Membrane	CSM RE 2540-BE	RO: CSM RE 2540-BE NF: CSM NE2540-70
Supplier	CSM	CSM
Membrane Type	Polyamide Thin-Film Composite	Polyamide Thin-Film Composite
Reported Salt Rejection (NaCl)	99.8%	RO: 99.8% NF: 40-70%
Permeability	$9.37 \cdot 10^{-12}$ m/s·Pa (0.137 gfd/psi)	RO: $9.37 \cdot 10^{-12}$ m/s·Pa (0.137 gfd/psi) NF: $1.34 \cdot 10^{-11}$ m/s·Pa (0.195 gfd/psi)
Maximum Operating Temperature	45 ºC	45 ºC
Maximum Operating Pressure	4127 kPa (600 psi)	4127 kPa (600 psi)
Maximum Feed Flow Rate	1.36 m^3/min (6 gpm)	1.36 m^3/min (6 gpm)
Minimum Feed Flow Rate	0.23 m^3/min (1 gpm)	0.23 m^3/min (1 gpm)
Maximum SDI	5	5

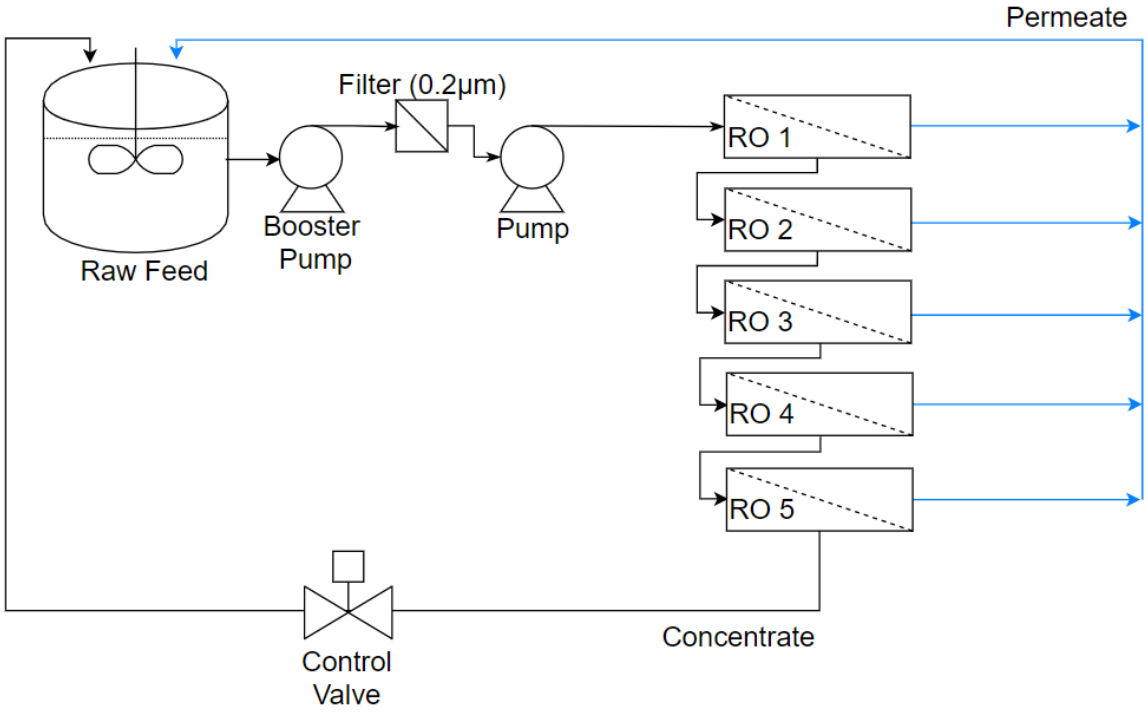

Figure 4.3. Process flow diagram of the experimental single-stage RO system (RO).

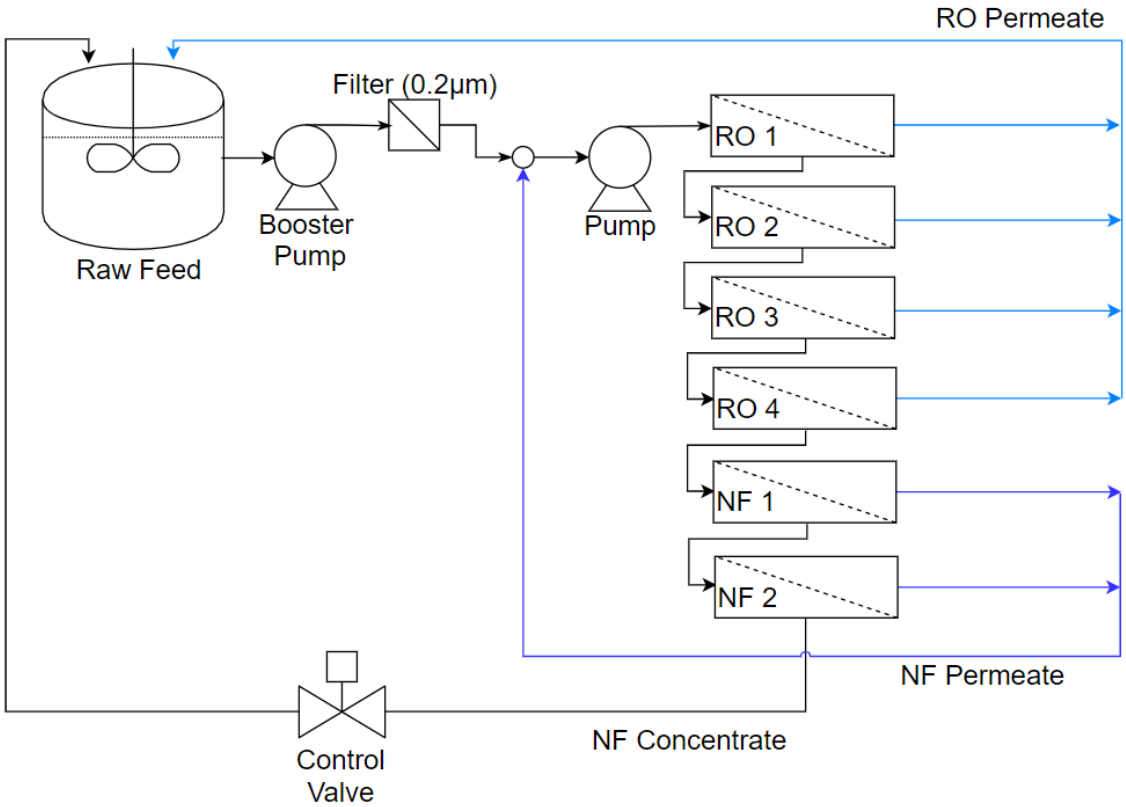

Figure 4.4. Process flow diagram of the experimental RO and NF hybrid system (RO-NF).

4.2.2. Model Solution

Desalination experiments were conducted using an aqueous 3,000 mg/l NaCl (Fisher Scientific, Massachusetts) solution. The solution was continuously mixed in the 379 L (100 gallon) feed tank with a portable mixer (NEP: A-1.0, Neptune Mixer Company, Pennsylvania). The composition and specification of the model solution are provided in Table 4.5.

Table 4.5. The model solution composition and specification.

Analytes	Concentration	Unit
Na^+	51.33	mM
Cl^-	51.33	mM
TDS	3000	mg/L
pH	7	
Osmotic pressure	2.39	bar (34.7 psi)

4.2.3. RO-NF Experiments

In both the RO and RO-NF system configurations, the experiments were conducted over RO permeate flux range of 0.017-0.0238 $m^3/m^2 \cdot hr$ (10-14 gfd). Utilizing an actuated valve at the end of the series of elements, the RO permeate flux was maintained at a prescribed value for a range of feed flow rates and feed pressure. While maintaining the RO permeate flux constant, the feed flow rate and applied pressure were adjusted to operate the system at a total recovery ranging from 40% to 90%. The feed flow rate ranged from 4,126 to 9,615 cm^3/min (1.09-2.54 gpm), and the RO feed pressure ranged from 1,172 to 2,489 kPa (170-361 psi). The applied pressure, feed flow rate, and recovery ranges for each configuration for the different RO permeate flux levels are shown in Table 4.6.

Table 4.6. The applied pressure, feed flow rate and recovery for RO permeate flux range of 0.017-0.0238 $m^3/m^2 \cdot hr$ (10-14 gfd).

Configuration/ RO Permeate flux	Applied pressure range	RO Feed range	Recovery range
RO / 0.017 $m^3/m^2 \cdot hr$ (10gfd)	1310-1827 kPa (190-265 psi)	4126-9161 cm^3/min (1.09-2.42 gpm)	40-86 %
RO / 0.0204 $m^3/m^2 \cdot hr$ (12gfd)	1517-2158 kPa (220-313 psi)	4656-9501 cm^3/min (1.23-2.51 gpm)	45-88 %
RO / 0.0238 $m^3/m^2 \cdot hr$ (14gfd)	1806-2489 kPa (262-361 psi)	5300-9350 cm^3/min (1.40-2.47 gpm)	54-90 %
RO-NF / 0.017 $m^3/m^2 \cdot hr$ (10gfd)	1172-1834 kPa (170-266 psi)	5224-8820 cm^3/min (1.38-2.33 gpm)	40-88 %
RO-NF / 0.0204 $m^3/m^2 \cdot hr$ (12gfd)	1413-1924 kPa (205-279 psi)	5716-9236 cm^3/min (1.51-2.44 gpm)	48-87%
RO-NF / 0.0238 $m^3/m^2 \cdot hr$ (14gfd)	1655-1979 kPa (240-287 psi)	6511-9615 cm^3/min (1.72-2.54 gpm)	57-82 %

5. Results and Discussion

5.1. NFF-FFR Experimental Results

In the multi-cycle NFF-FFR operation, raw data were acquired every ten seconds. The data were normalized based on the initial operational data (i.e., operational data at the beginning of the experiment) (Appendix C.2). The feed flow rate and recovery were fixed at 8637.6 cm^3/min (1.9 gpm) and 65%, respectively. The feed water contained 10 mM of sodium chloride and 10 mM of calcium sulfate, with 2,024 mg/L total dissolved solids (TDS). The gypsum saturation index (SI) of the feed and retentate streams were 0.52 and 1.64, respectively.

The permeability of the monitored membranes were determined as per Eq. (8) $\left(L_p = \frac{J_v}{\Delta P - \Delta \pi}\right)$, and the scaling surface coverage was analyzed in MMD following the methodology discussed in Appendix C.3. Feed flow reversal (FFR) was triggered when the surface scale coverage of MMD reached 6%. This scaling threshold was equivalent to about 2.5% flux decline in the monitored element. FFR was operated for the same duration as for normal feed flow (NFF) operation, then the operation was switched to NFF mode. Figure 5.1 shows the normalized permeability and surface scale coverage in the MMD for a single cycle over a period of 11 hours.

During NFF operation, the monitored element permeability was expected to decrease, because the element was exposed to the highest level of gypsum saturation. The saturation index of gypsum (SI_g) of the concentrate was at 1.64 (determined using the OLI software). The gypsum saturation index at the surface of the spiral-wound RO membrane ($SI_{g,m}$) was higher than the gypsum saturation index of the RO retentate due to concentration polarization (CP). The CP factor was determined via Eq. (18), and confirmed via the CSM RO process simulation software (CSMPRO v5.0, Toray Advanced Materials, Korea).

The permeability of the monitored membrane decreased with increased surface scaling and

scale removal was achieved via FFR. $SI_{g,m}$ in MMD was slightly higher than $SI_{g,m}$ in the spiral-wound element, though they were exposed to the same feed concentration. This was due to the absence of a channel spacer in the MMD. Without a channel spacer, the CP was higher in MMD than the spiral-wound membrane element. It is noted that channel spacer induces flow instabilities (resulting in a level of mixing) near the membrane surface which lowers the scaling potential. The $SI_{g,m}$ in MMD without a channel spacer was 2.05, as estimated via the Graetz-Lévêque equation (Appendix B.3).

During feed flow reversal (FFR) operation, the spiral-wound element permeability was partially recovered. As the monitored tail element became the lead element upon FFR, the tail membrane element was exposed to the undersaturated feed water, for which SI_g was 0.52. At this SI_g and at the CP value of 1.02, the $SI_{g,m}$ in the spiral wound element was determined to be 0.53. At the above $SI_{g,m}$, gypsum crystals that formed on the membrane surface rapidly dissolved, the active membrane surface area was restored, and the membrane permeability was recovered.

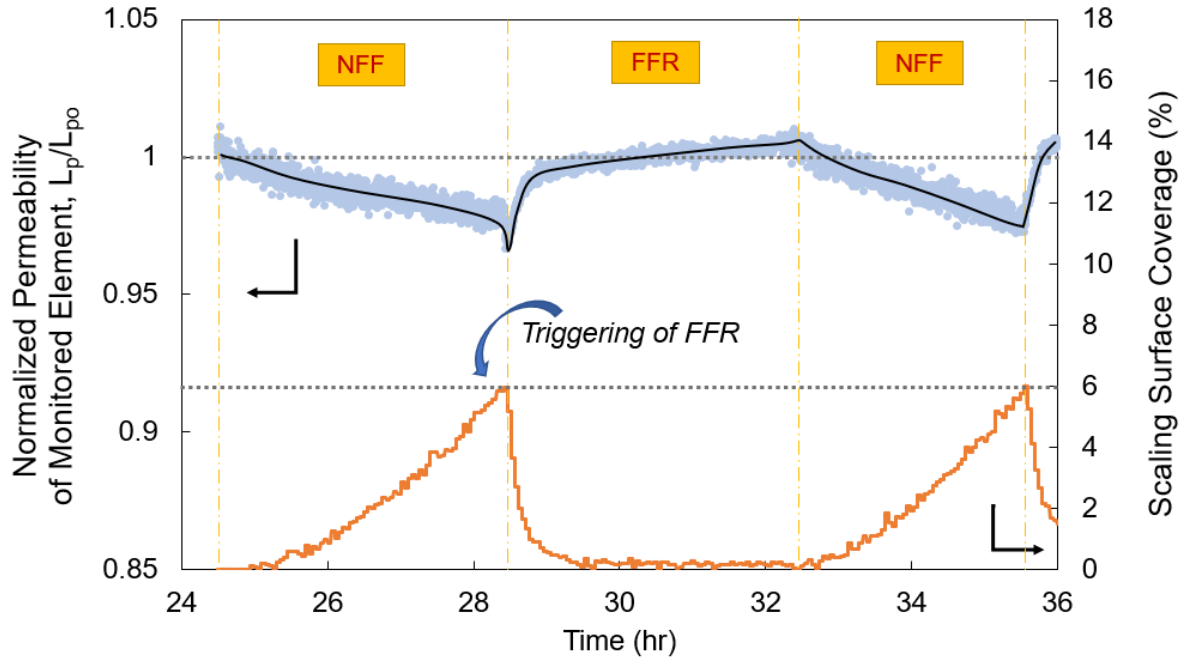

Figure 5.1. Normalized permeability of the tail element during single NFF-FFR cycle and surface scale coverage. Triggering of FFR was carried out when surface scale coverage reached 6%. Operating conditions: feed flow rate = 8637.6 cm^3/min (1.9 gpm), feed pressure = 1,407 kPa (204 psi), recovery = 65%, SI_{gypsum} of the feed = 0.52.

Evaluation of multi-cycle NFF and FFR operation was carried out for 44 hours. Subsequently, the system was flushed with DI water for 45 hours. After DI water flushing, the experiment continued for another 40 hours. The feed flow rate and pressure was at 8,637.6 cm^3/min (1.9 gpm) and 1,407 kPa (204 psi), and the recovery was set to 65%. The raw data were acquired every ten seconds, and the values were then averaged over about 30 minute intervals. The normalized permeability of the monitored membrane and surface scale coverage in the MMD during the multi-cycle between NFF and FFR operation are shown in Figure 5.2. The permeability of the monitored element decreased during NFF operation, which corresponded to the increase in surface scale coverage. During FFR operation, surface scale coverage decreased while the monitored element permeability partially recovered (~97.5% during six cycles).

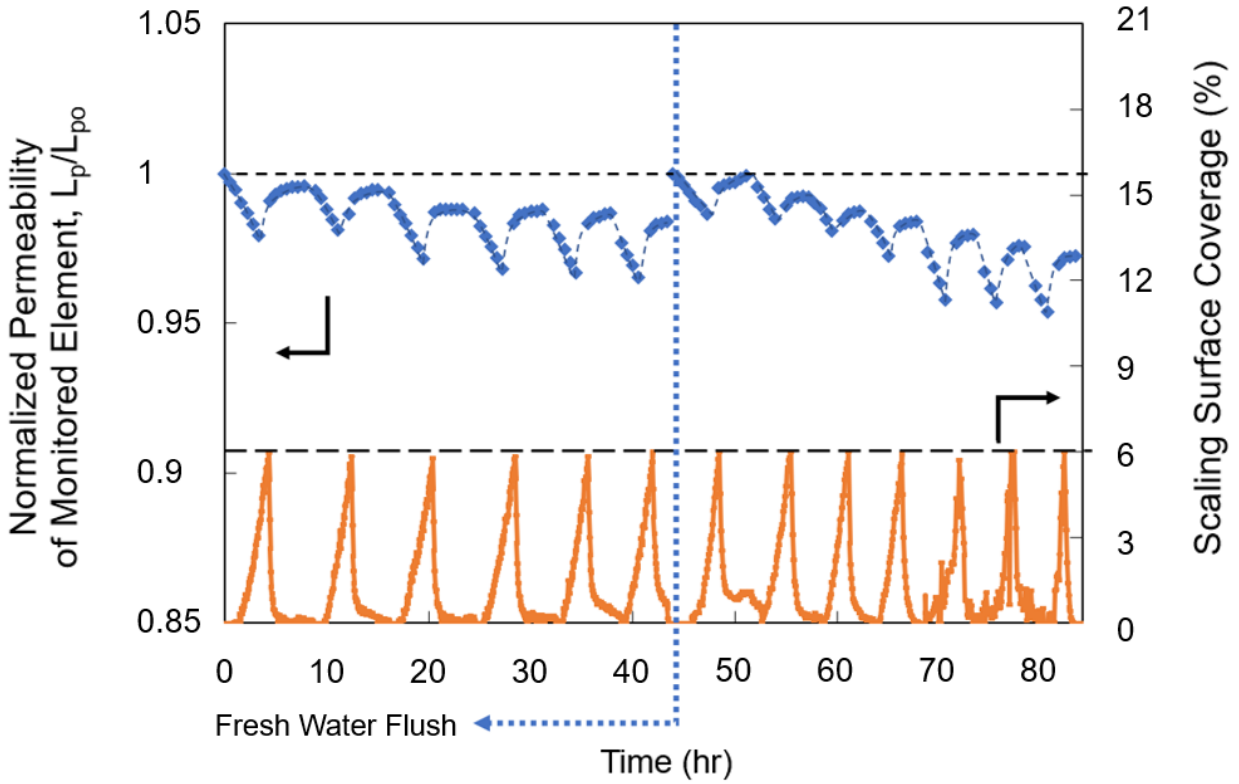

Figure 5.2. Normalized permeability of the tail element (Appendix C.2) during multiple NFF-FFR cycles, presented with the surface scale coverage. Fresh water flushing was carried out after 45 hours of operation. (Lp_o: initial permeability of the monitored element). Operating conditions: feed flow rate = 8637.6 cm^3/min (1.9 gpm), feed pressure = 1407 kPa (204 psi), recovery = 65%, SI_{gypsum} of the feed = 0.52.

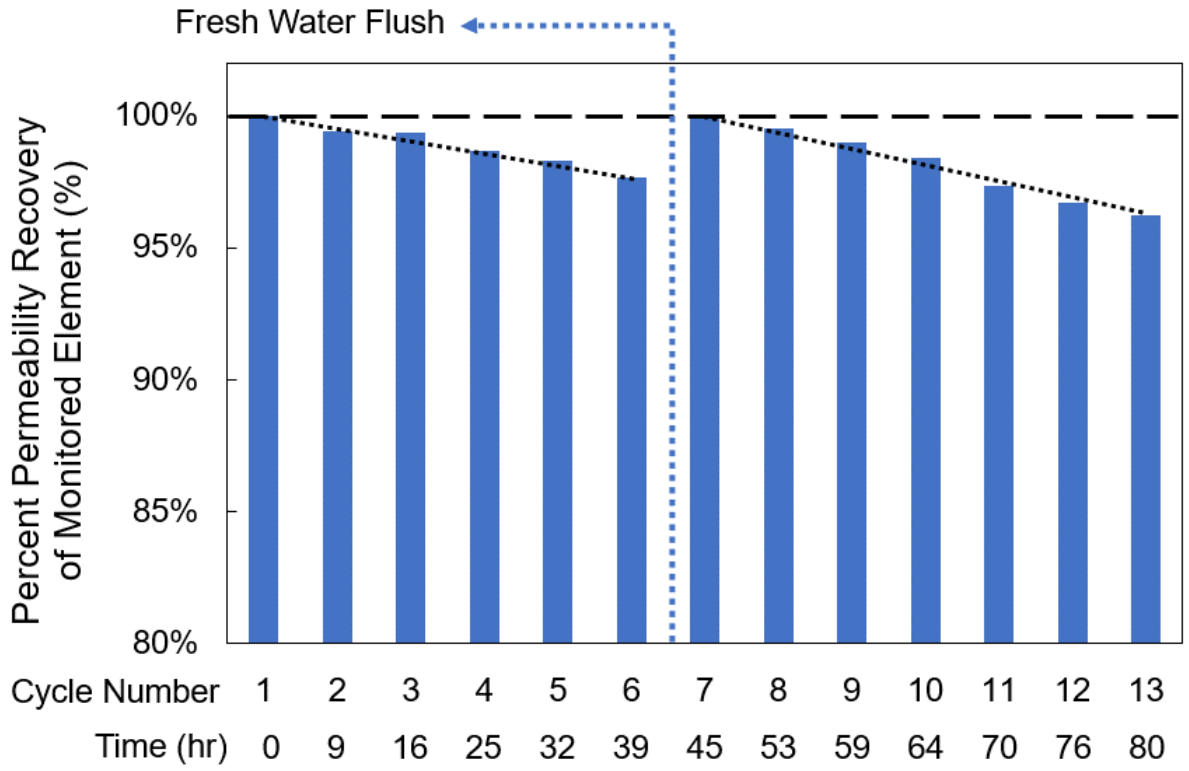

Figure 5.3. Permeability recovery (%) of the monitored element for multiple cycles. Fresh water flushing was carried out between cycles 6 and 7. Operating conditions: feed flow rate = 8637.6 cm^3/min (1.9 gpm), feed pressure = 1407 kPa (204 psi), recovery = 65%, SI_{gypsum} of the feed = 0.52.

The percent permeability recovery of the monitored membrane for each NFF-FFR cycle is shown in Figure 5.3. The percent permeability recovery for the first six cycles was determined based on the permeability of the membrane immediately after the beginning of NFF operation (L_p) relative to the initial permeability of the monitored membrane in the first cycle (L_{po}). After cycle 6 the RO system was freshwater flushed for 45 hours at 2728 cm^3/min (0.6 gpm) of DI water at 262 kPa (38 psi). For the next seven cycles, the percent permeability recovery of the monitored membrane was assessed relative to the initial permeability of the membrane in NFF operation in the first cycle. Over the operational period of 43 hrs, the permeability decrease was about 2.5% for the first six cycles. After freshwater flush at t=43 hr, over the subsequent period of 40 hrs, the

decrease in permeability was about 3.8% for the subsequent seven NFF/FFR cycles. As the cycles proceeded, the percent permeability recovery decreased due to incomplete dissolution of the formed scale crystals in the spiral-wound RO membrane. The above results suggest that for the level of feed saturation with respect to gypsum, the driving force for complete dissolution was insufficient when the transition from NFF to FFR is triggered at MMD surface scale coverage of 6%. In order to alleviate the above limitation, one could trigger FFR at a lower level of MMD surface scale coverage, though this would require higher frequency of FFR/NFF switching.

Images of the membrane surface in the MMD during NFF and FFR operation are shown in Figure 5.4. These images for NFF/FFR cycle 3 are for the growth of gypsum crystals during the NFF operation over the period of three hours (image (a), (b), and (c)). For the specific example shown in Figure 5.4, surface scale coverage reached the FFR triggering threshold (i.e., 6% scale coverage in MMD) after 3 hours and 5 minutes of NFF operation. Dissolution of gypsum crystal is shown in images (e) and (f) over a period of one hour.

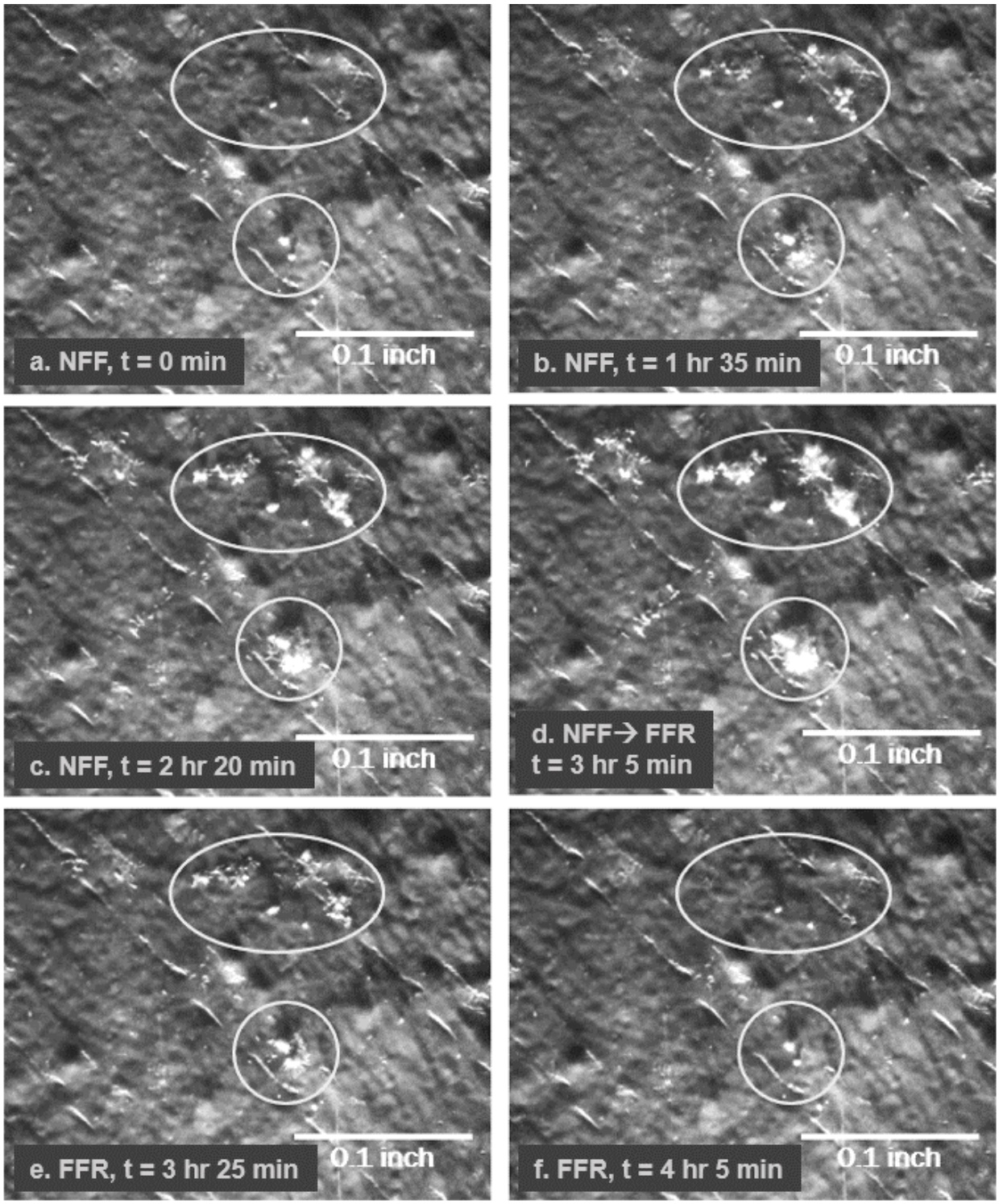

Figure 5.4. Images of the RO membrane surface obtained in MMD during normal feed flow (NFF) and feed flow reversal (FFR) cycle 3. The growth of the gypsum crystals during NFF operation is shown in images (a)-(d). The dissolution of the gypsum crystals upon FFR is shown in images (e) and (f). Operating conditions: feed flow rate = 8637.6 cm^3/min (1.9 gpm), feed pressure = 1407 kPa (204 psi), recovery = 65%, SI_{gypsum} of the feed = 0.52.

In order to quantify the kinetics of crystal dissolution, a number of different gypsum crystals were selected from MMD images. During FFR operation, gypsum crystals that formed on the membrane surface during NFF were dissolved as they were exposed to the undersaturated feedwater. The change in equivalent crystal radius for the selected crystals over the course of FFR is shown in Figure 5.5.

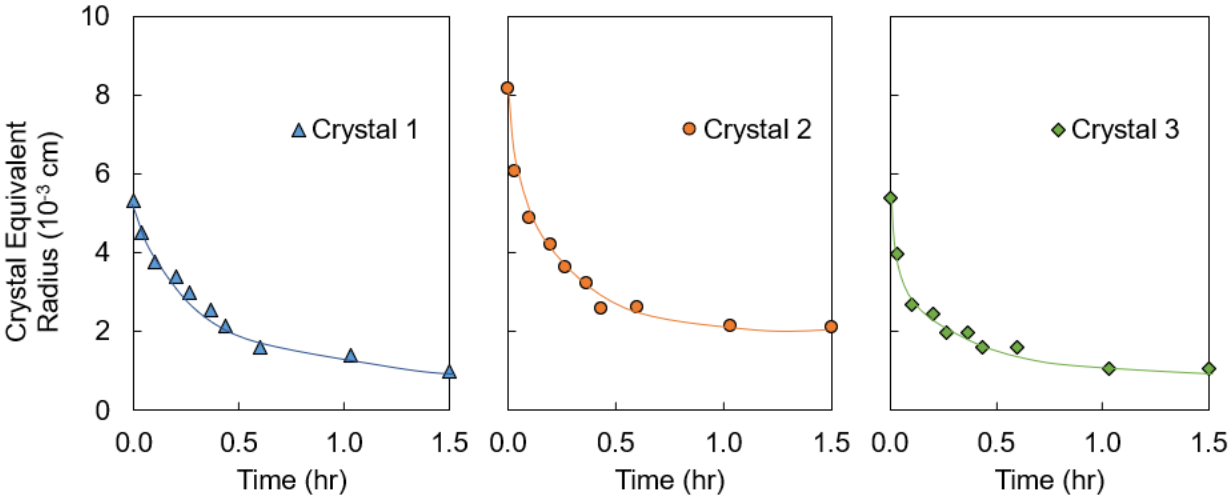

Figure 5.5. Surface area of selected gypsum crystals observed via MMD during feed flow reversal (FFR) cycle 3. Operating conditions: feed flow rate = 8637.6 cm^3/min (1.9 gpm), feed pressure = 1407 kPa (204 psi), recovery = 65%, SI_{gypsum} of the feed = 0.52.

For the initial period of crystal growth (up to about 0.5 hours) the log plot of normalized crystal surface area (A/A_o, where A is crystal surface area at time t and A_o is crystal surface area at t=0) is shown in Figure 5.6. The overall trend (considering the three different crystals) is of the form $\ln(A/A_o) = at$ where a = -5.4 hr^{-1} (i.e., slope of the trendline). The dissolution rate of gypsum crystals are shown in Figure 5.7. The larger crystal dissolves faster compared to the smaller crystals, since the of crystal dissolution is proportional to the crystal equivalent radius [24]. While there were some differences in the rate of dissolution depending on the initial crystal size, dissolution was rapid within the first ½ hour leading to nearly complete removal of the formed crystal. It is noted

that crystals form at different times during the RO process as crystal nucleation is a stochastic process. Therefore, the rate of scale removal during NFF is governed by the large crystals.

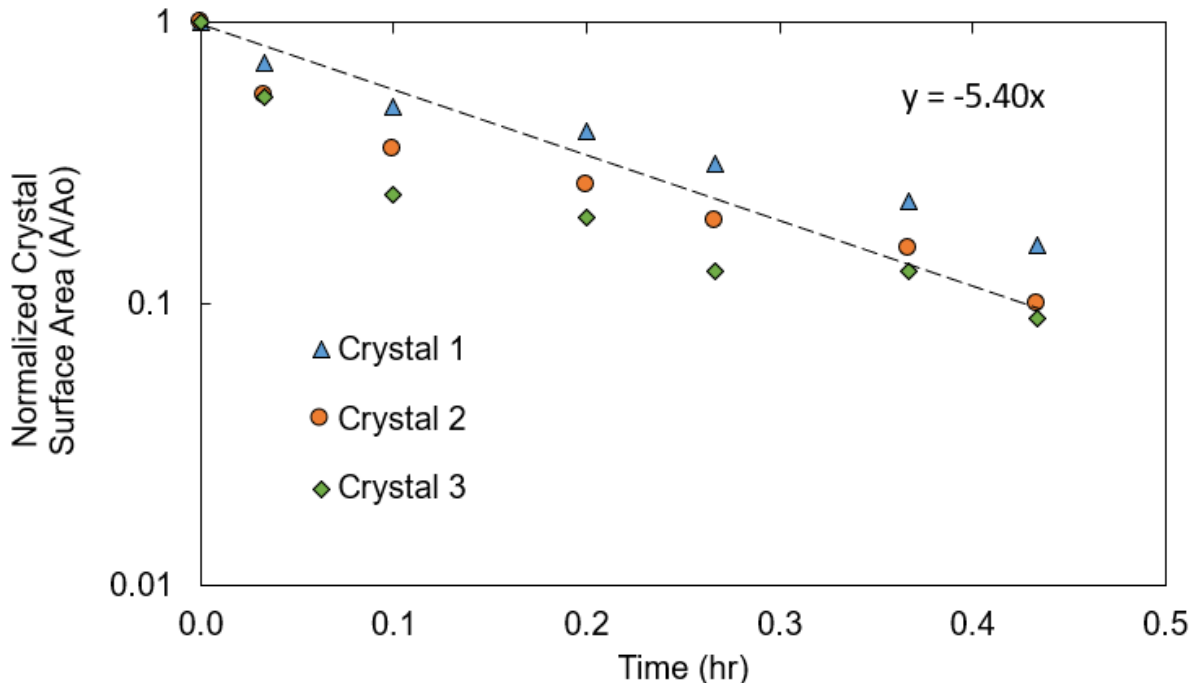

Figure 5.6. Dissolution rate of selected gypsum crystals observed via MMD during feed flow reversal (FFR) cycle 3 (Figure 5.2). The initial equivalent crystal radii for crystals 1, 2, and 3 were $5.3 \cdot 10^{-3}$ cm, $8.1 \cdot 10^{-3}$ cm, and $5.4 \cdot 10^{-3}$ cm, respectively. Operating conditions: feed flow rate=8,637.6 cm^3/min (1.9 gpm), feed pressure = 1,407 kPa (204 psi), recovery = 65%, SI_{gypsum} of the feed = 0.52.

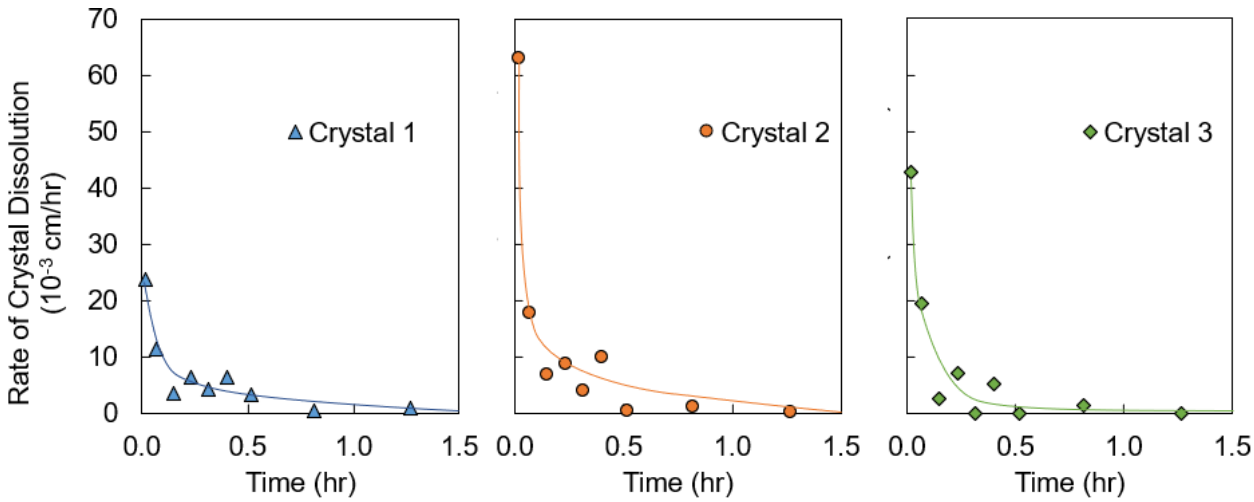

Figure 5.7. Dissolution rate of selected gypsum crystals observed via MMD during feed flow reversal (FFR) cycle 3 (Figure 5.2). The initial equivalent crystal radii for crystals 1, 2, and 3 were $5.3 \cdot 10^{-4}$ cm, $8.1 \cdot 10^{-4}$ cm, and $5.4 \cdot 10^{-4}$ cm, respectively. Operating conditions: feed flow rate=8,637.6 cm^3/min (1.9 gpm), feed pressure = 1,407 kPa (204 psi), recovery = 65%, SI_{gypsum} of the feed = 0.52.

5.2. RO and RO-NF Experiments

Desalting experiments with the RO (five RO elements, single pass) and RO-NF (four RO elements and two NF elements, single pass) configurations were conducted over permeate flux range of 0.017-0.0238 $m^3/m^2 \cdot hr$ (10-14 gallons per sq. ft. per day (gfd)). In each experiment, the pressure requirements for desalting feed water of 3,000 ppm TDS (NaCl solution) was determined for a total recovery operation in the range of 40% to 90% at a fixed overall RO permeate flux.

5.2.1. Series of Five RO Experiment Result

The applied pressure, normalized with respect to the feed osmotic pressure (2.4 bar (34.7 psi)), for permeate flux in the range of 0.017-0.0238 $m^3/m^2 \cdot hr$ (10-14 gfd), along with the predictions for operations up to the crossflow thermodynamic restriction (Eq. (20), Section 2.3.1) are shown in Figure 5.8.

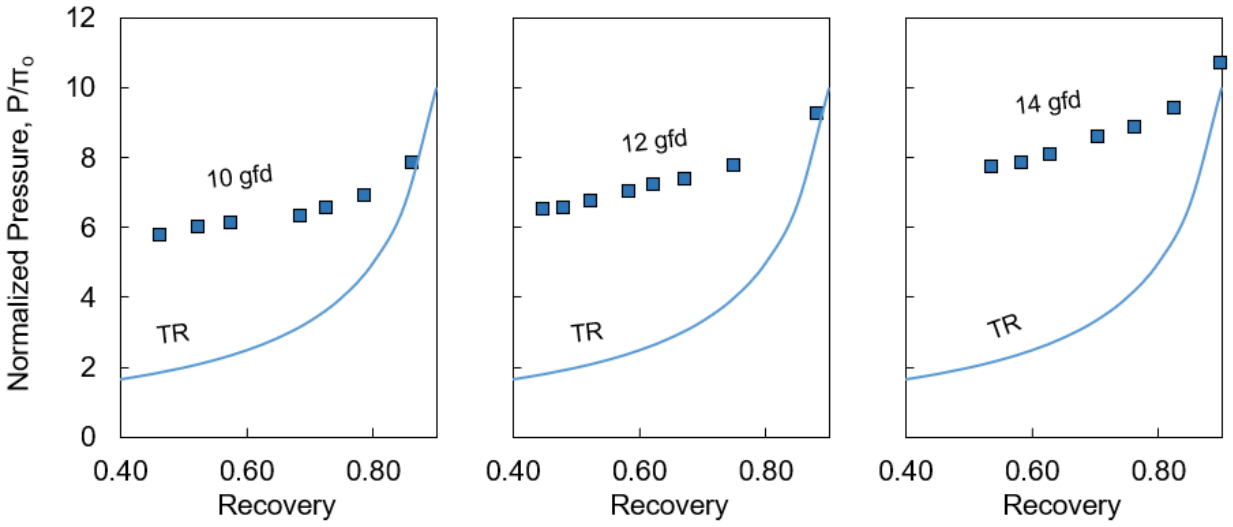

Figure 5.8. Normalized pressure versus recovery for 0.017, 0.0204, and 0.0238 $m^3/m^2 \cdot hr$ (10, 12, and 14 gfd) permeate flux for RO configuration of five RO membrane elements in series. The applied pressures were normalized based on the feed osmotic pressure 2.4 bar (34.7 psi). Also shown are the predictions for operation up to the thermodynamic restriction (TR) limit (Eq. (20)).

At a fixed RO permeate flux, the recovery increased as the applied pressure increased. The applied RO feed pressure range was 1,310-2,489 kPa (190-361 psi) and the RO feed flow rate was in the range of 4,126-9,501 cm^3/min (1.09-2.51 gpm). Also, since the membrane active area was fixed, higher feed pressure and feed flow rate were required as the RO permeate flux increased. In all cases, the normalized applied pressure was significantly higher relative to the ideal operation at the thermodynamic restriction. This is not surprising since the 5 RO elements in series in the current RO system was insufficient to reach the thermodynamic limit at the system tail element exit (i.e., where the retentate osmotic pressure matches the applied pressure).

The specific energy consumption (SEC) and the normalized SEC (Eq. (25), $NSEC = \frac{1}{Y_{RO}}\left(\frac{p_f}{\pi_o}\right)$) versus recovery are shown in Figures 5.9 and 5.10, respectively. The data suggests that for the current RO system and the range of tested product water recovery, there is an optimal recovery (81%, 82%, and 84% for 0.017, 0.0204, and 0.0238 $m^3/m^2 \cdot hr$) at which the energy consumption is at minimum.

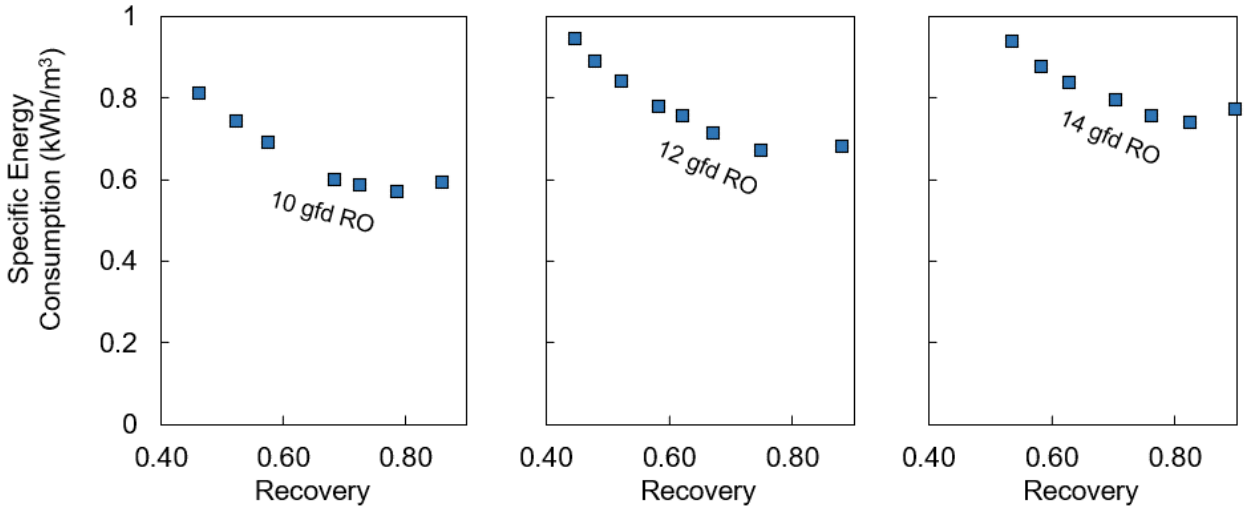

Figure 5.9. Specific energy consumption (SEC) versus recovery for 0.017, 0.0204, and 0.0238 $m^3/m^2 \cdot hr$ (10, 12, and 14 gfd) permeate flux for RO configuration of five RO membrane elements in series. The specific energy consumption utilization for desalting in the RO elements was calculated as per Eq. (24).

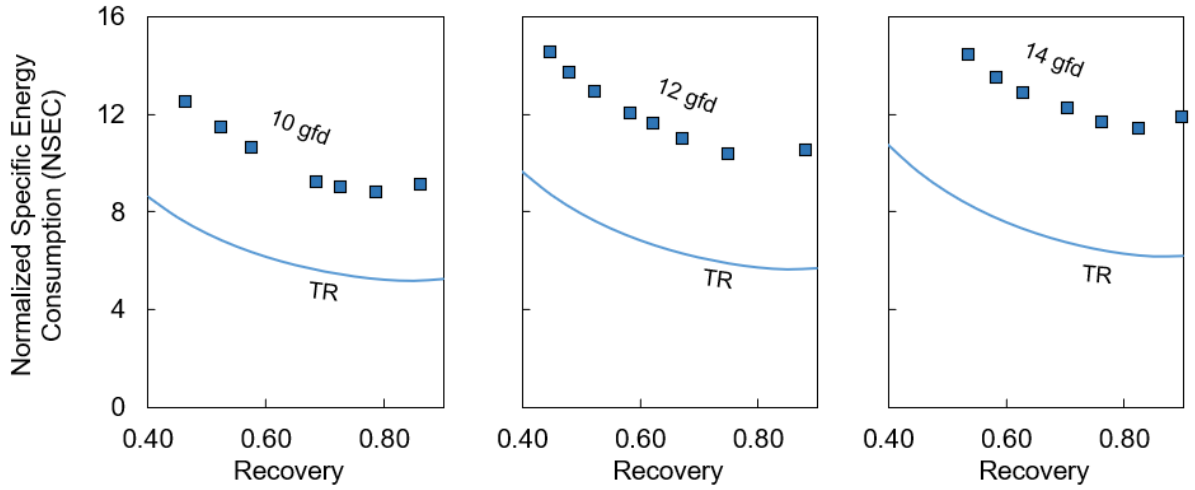

Figure 5.10. Normalized specific energy consumption versus recovery for permeate flux of 0.017, 0.0204, and 0.0238 $m^3/m^2 \cdot hr$ (10, 12, and 14 gfd) for RO system configuration of five RO membrane element system. Also shown are the normalized specific energy consumption for desalting in the RO elements as per Eq. (25) and the prediction for operation up to the thermodynamic restriction (TR) limit (Eq. (29)).

5.2.2. RONF Hybrid Experiment Result

The RO-NF experiments were conducted for a system configuration of four RO membrane elements in series followed by two NF elements in series. The main function of the RO stage is to provide the main function of desalting water, while the NF stage serves to minimize the concentrate volume and recycle the NF permeate to the RO feed (Figure 3.5). As discussed in Section 2.3.2, the pressure requirement for the RO-NF configuration was lower than that for the RO configuration, over the recovery range of 40% to 85%. The differences in required pressure for the RO and RO-NF configurations were greatest for 0.0238 $m^3/m^2 \cdot hr$ (14 gfd). The above results suggest that, for the evaluated recovery and permeate flux ranges, the RO-NF configuration can be effectively utilized to overcome the feed pressure barrier.

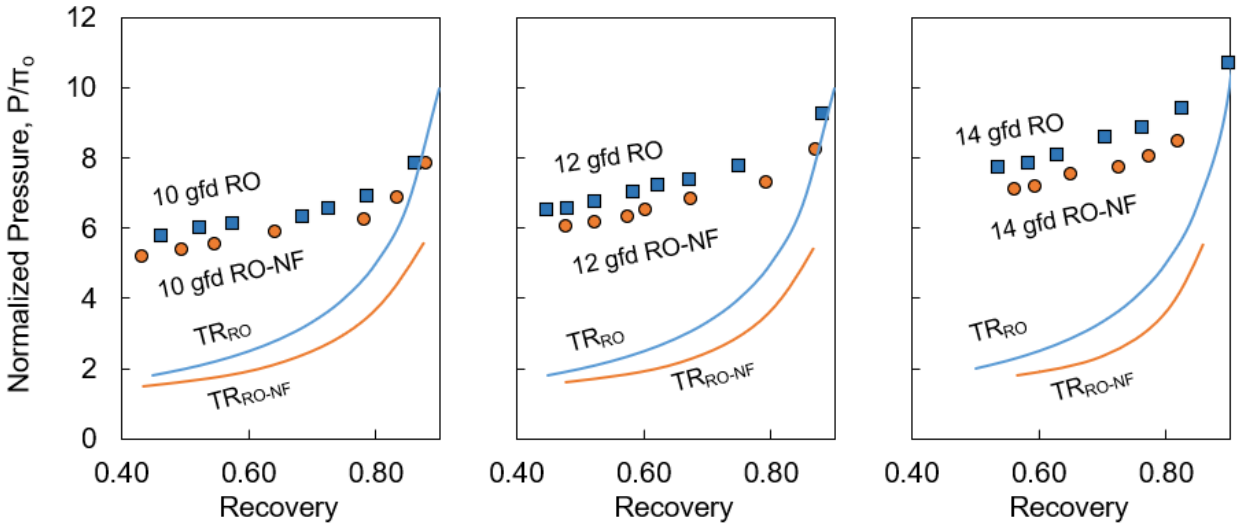

Figure 5.11. Plots of normalized pressure versus recovery for permeate flux of 0.017, 0.0204, and 0.0238 $m^3/m^2 \cdot hr$ (10, 12, and 14 gfd) for system configuration of five RO elements in series and for a hybrid RO-NF system of 4 RO elements in series followed by 2 NF elements in series. The applied pressures were normalized based on the feed osmotic pressure of 2.4 bar (34.7 psi). The normalized pressure ($=P_{RO}/\pi_f$) as predicted for operation up to the thermodynamic restriction (TR) limit is also shown for both the RO (Eq. (20)) and RO-NF (Eq. (38)) operations, respectively.

The normalized feed pressure ($=P/\pi_o$) per recovery for both RO and RO-NF configurations are shown in Figure 5.11, and the thermodynamic restrictions of each configurations are also plotted. Since the thermodynamic restrictions of RO-NF configurations are dependent on intrinsic rejection of RO and NF membranes, it was plotted based on the experimental data. It is clear that the thermodynamic restrictions of processes in RO-NF configuration are lower than that of processes in RO configuration, at a given recovery and RO permeate flux. Also, it is observed that at extreme recovery (0.017 $m^3/m^2 \cdot hr$ (10 gfd), Y=88%), the normalized pressure in RO-NF configuration is lower than the thermodynamic restrictions of process in RO configuration.

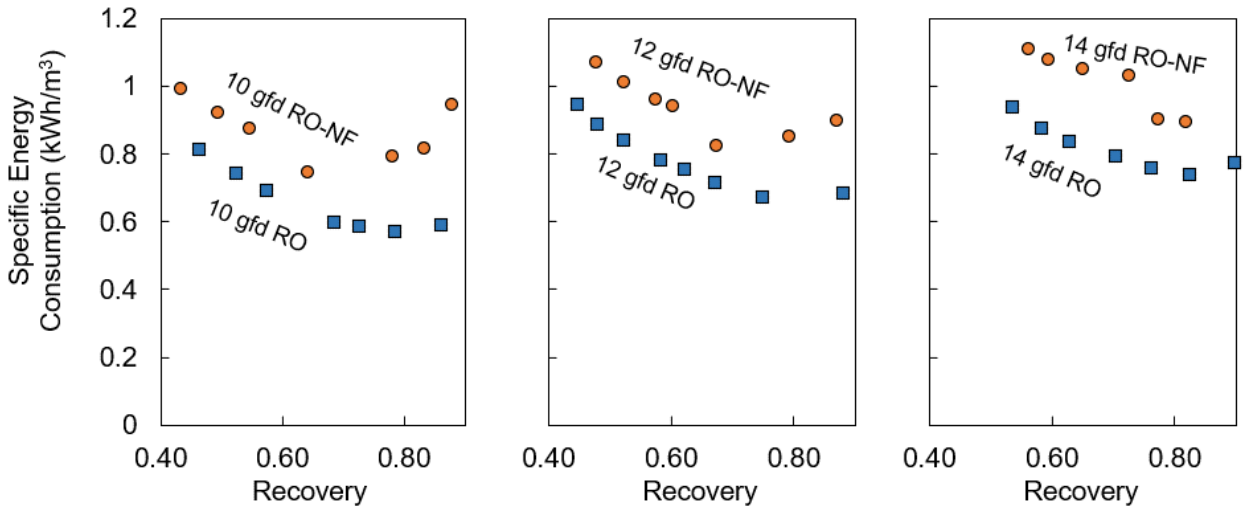

Figure 5.12. Specific energy consumption (SEC) versus recovery for permeate flux of 0.017, 0.0204, and 0.0238 $m^3/m^2 \cdot hr$ (10, 12, and 14 gfd) for system configuration of five RO elements in series and for a hybrid RO-NF system of 4 RO elements in series followed by 2 NF elements in series. The SEC for desalting in the RO elements was calculated as per Eq. (24).

The specific energy consumption versus recovery for 0.017, 0.0204, and 0.0238 $m^3/m^2 \cdot hr$ (10, 12, and 14 gfd) RO permeate flux for both RO and RO-NF configurations are shown in Figure 5.12. It is noted that within the range of recovery and RO permeate flux in this study, the SEC of process in RO configuration are about 10-20% lower than that of RO-NF configuration. This indicates that more energy is consumed if the process is in RO-NF configuration than RO configuration.

The plots of normalized specific energy consumption (NSEC) versus recovery for the different RO permeate fluxes are shown in Figure 5.13. The minimum NSEC occurred at recovery of 78%, 82%, 80%, for 0.017, 0.0204, and 0.0238 $m^3/m^2 \cdot hr$ (10, 12, and 14 gfd) RO permeate flux, respectively. Although the thermodynamic restrictions of both RO and RO-NF configurations are similar, the experimental results show that the RO-NF requires higher degree of energy consumption when compared to RO configuration, within RO permeate flux range of 0.017-0.0238 $m^3/m^2 \cdot hr$ (10-14 gfd) and recovery range of 40-90%.

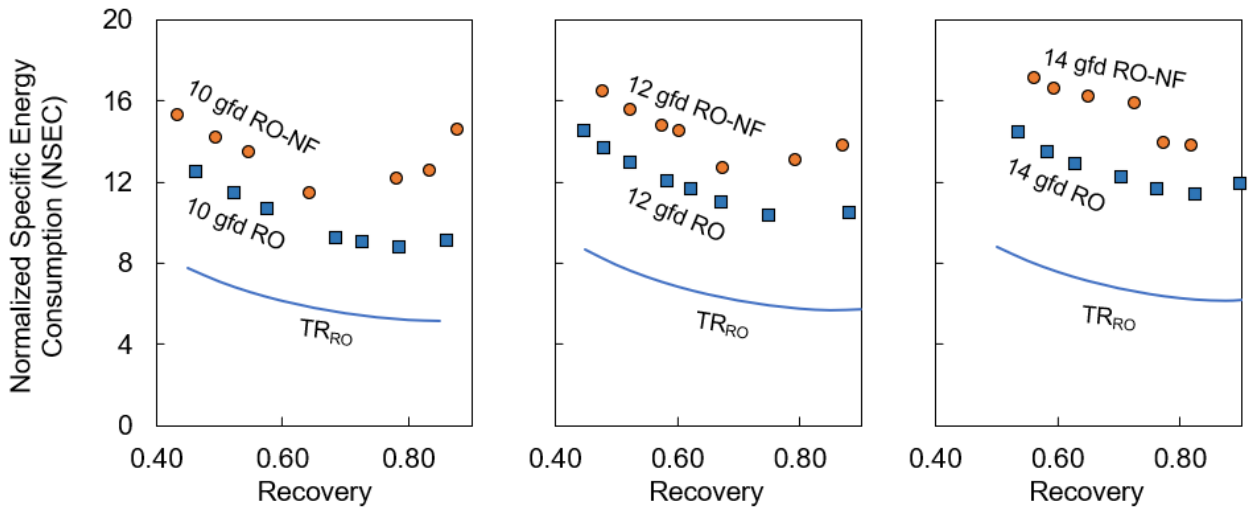

Figure 5.13. Plots of normalized specific energy consumption (Eq. (25)) versus recovery for permeate flux of 0.017, 0.0204, and 0.0238 $m^3/m^2 \cdot hr$ (10, 12, and 14 gfd) for system configuration of five RO elements in series and for a hybrid RO-NF system of 4 RO elements in series followed by 2 NF elements in series. Also shown are the predictions for operation up to the thermodynamic restriction (TR) limit for RO desalting (Eq. (29)).

6. Conclusions and Recommendations

6.1. Conclusions

The operation of RO desalting in the mode of feed flow reversal was evaluated in a series of experiments to assess the potential of the approach to reduce membrane scaling. Subsequently, the possibility of overcoming the feed pressure limitation in RO desalting was evaluated for a hybrid RO-NF configuration.

1. Conventional RO water desalination employs crossflow regime, and it is typical for the feed to flow in one direction (normal feed flow, NFF). With the objective of mitigating membrane surface scaling, feed that is sufficiently undersaturated can be periodically directed to flow in reverse direction (feed flow reversal, FFR). The periodic switch between these two operational modes is referred as NFF-FFR operation.
2. RO operation in the mode of cyclic NFF-FFR operation can partially mitigate excessive membrane scaling, while eliminating the use of costly antiscalant. In the present study with feed water of $SI_g = 0.6$, it was found that the permeability decline for operation in the mode of NFF/FFR was up to 2.5% over six cycles, whereas the length of each cycle was above 10 hours.
3. Periodic freshwater flush can be incorporated with FFR operation to enhance the overall process performance by removing undissolved membrane gypsum scale crystals.
4. At the same pressure, the recovery for RO-NF desalting was significantly higher, 20-30% relative to the recovery achieved in conventional RO over a recovery range of 40-90%. At the same recovery, the required feed pressure for RO-NF desalting was about 10-15% lower compared to conventional RO process configuration.
5. Although RO-NF process configuration is effective in lowering the required feed pressure

for given recovery, the specific energy consumption was about 5-15% higher relative to conventional RO process.

6.2. Recommendations

1. Triggering feed flow reversal (FFR) and the switch to normal feed flow (NFF) could be optimized with respect to the level of membrane scale coverage in the membrane monitoring.
2. The effective frequency of periodic freshwater flush should be studied, which aims to assist in complete dissolution of gypsum crystals with small effect to the overall productivity of the process.
3. The degree of pressure reduction of RO desalination process in RO-NF configuration at high recovery should be explored over a wider range of feed solution salinity and range of RO and NF membranes salt rejection.
4. The potential reduction in overall energy utilization via the use of energy recovery devices should be explored for the hybrid RO-NF process configuration.

Appendices

Appendix A. Calibration of Sensors in RO system

The flow meter sensors utilized in the RO system (Table 3.1, 3.2) were calibrated by comparing the sensor measurement with manual measurement. The standard solutions were used to calibrate the conductivity meters (Table 3.1, 3.2).

A.1. Flow meter calibration

Two types of flow meter were utilized in the RO system. The flow meters for the upper flow rate range, 0.2 - 12 gpm, (Signet 3-2537-1C, GF Piping Systems, California) were used for the feed, concentrate, and permeate streams (FT-1, FT-2, and FT-5). Flow meters for the lower flow rate range, 200-2,000 cm^3/min, (101 Liquid Flo-Sen, McMillan, Texas) were used for the permeate streams of the first and last RO elements (FT-3 and FT-4). Sensor readings were compared to manually measured flow rates, which was taken via recording the time for the effluent to fill a 1L graduated cylinder. The flow rates sensors calibration curves are provided in Figures A.1-A.5.

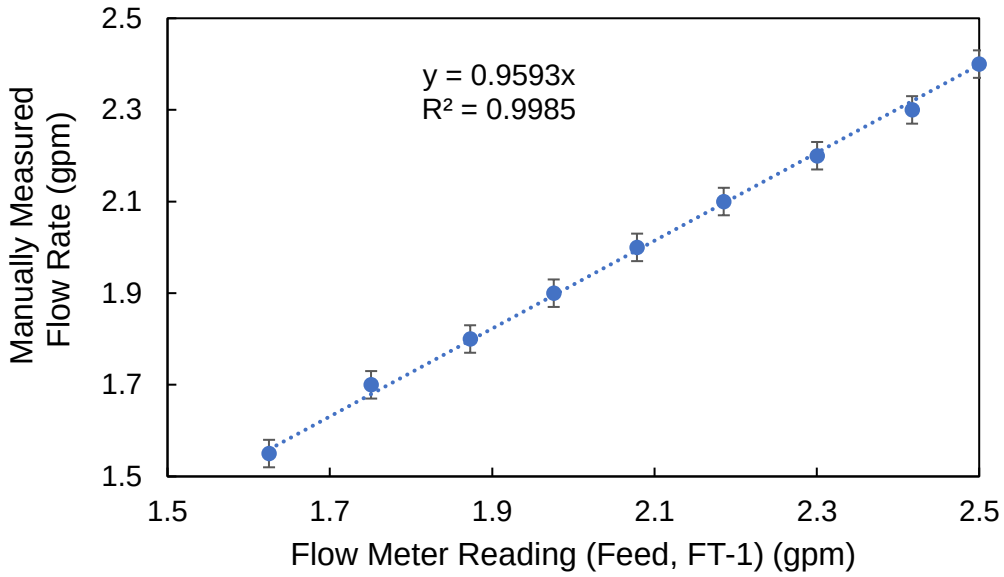

Figure A.1. Flow meter calibration curve for feed flow rate sensor (Signet 3-2537-1C, FT-1).

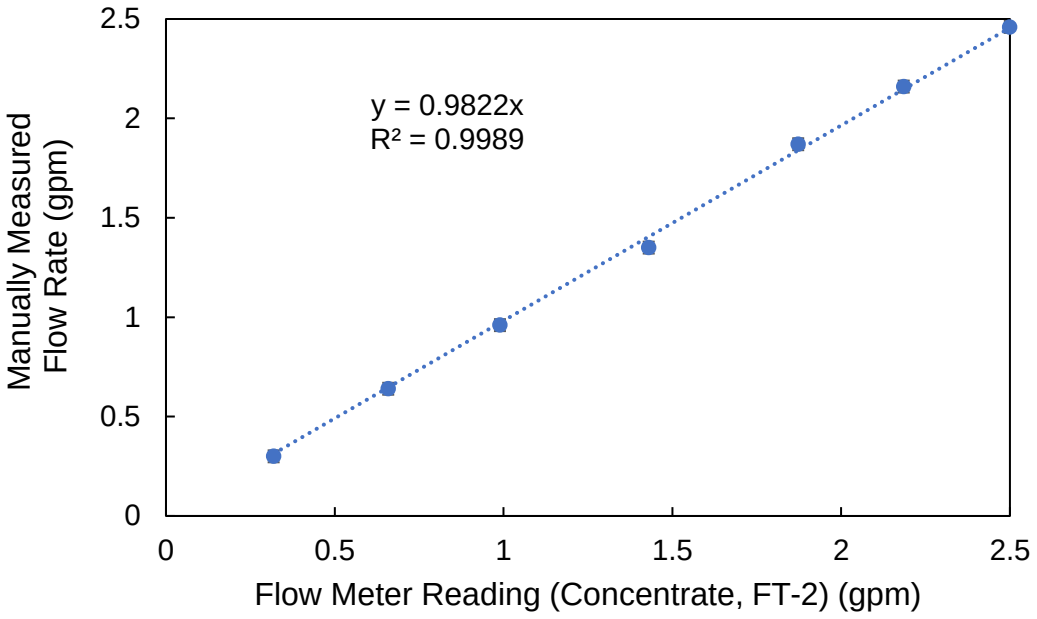

Figure A.2. Flow meter calibration curve for concentrate flow rate sensor (Signet 3-2537-1C, FT-2).

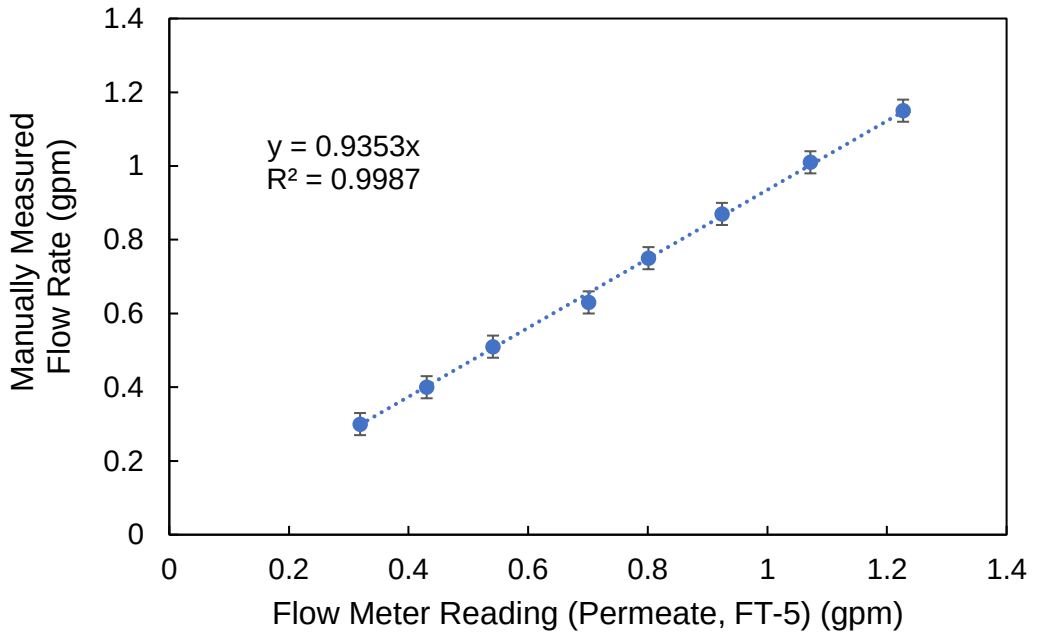

Figure A.3. Flow meter calibration curve for combined (total) permeate flow rate sensor (Signet 3-2537-1C, FT-5).

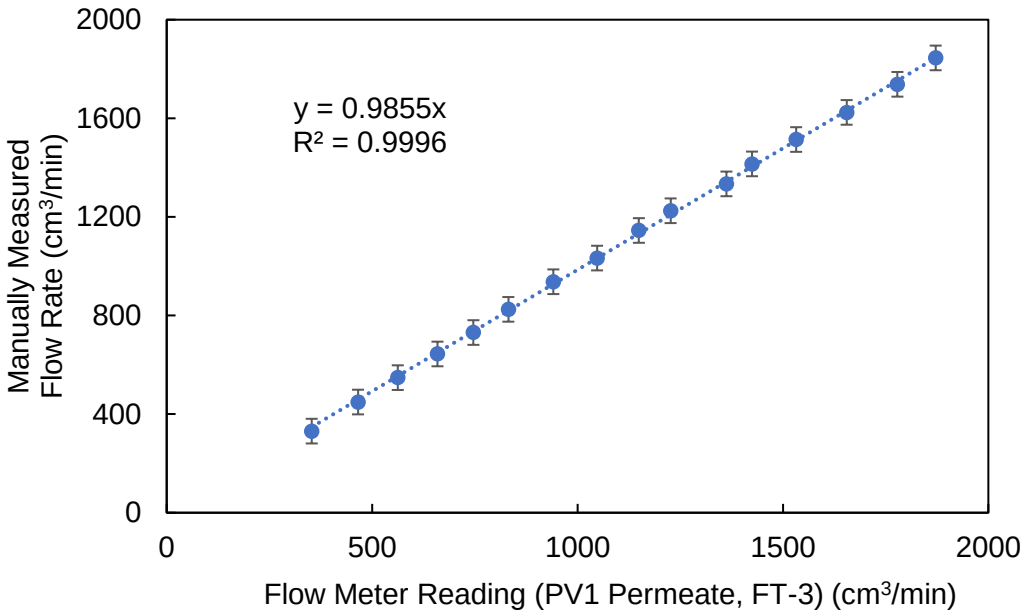

Figure A.4. Flow meter calibration curve for PV1 permeate flow rate sensor (101 Liquid Flo-Sen, FT-3).

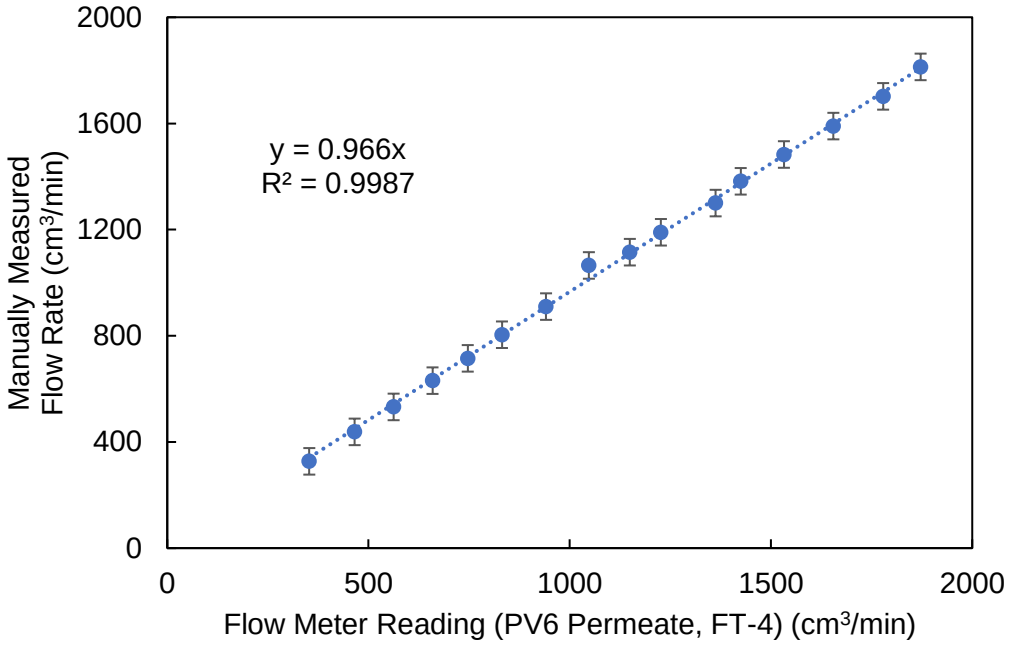

Figure A.5. Flow meter calibration curve for PV6 flow rate sensor (101 Liquid Flo-Sen, FT-4).

A.2. Conductivity meter calibration

The conductivity meters for the feed and concentrate had a range of 100 - 200,000 uS/cm (3-2850-52-42V, GF Signet, California), whereas the conductivity meter with a measurement range 0-10,000 uS/cm was used for the permeate steam (3-2850-52-41V, GF Signet, California). The calibration curve for the above sensors are shown in Figures A.6 and A.7. Standard conductivity calibration solutions of 84 uS, 447 uS, 1413 uS, and 80 mS (WD-00653-16, WD-00653-47, WD-00653-18, WD-00653-32, Oakton, Illinois) were used to compare the sensor readings and obtain correction factors.

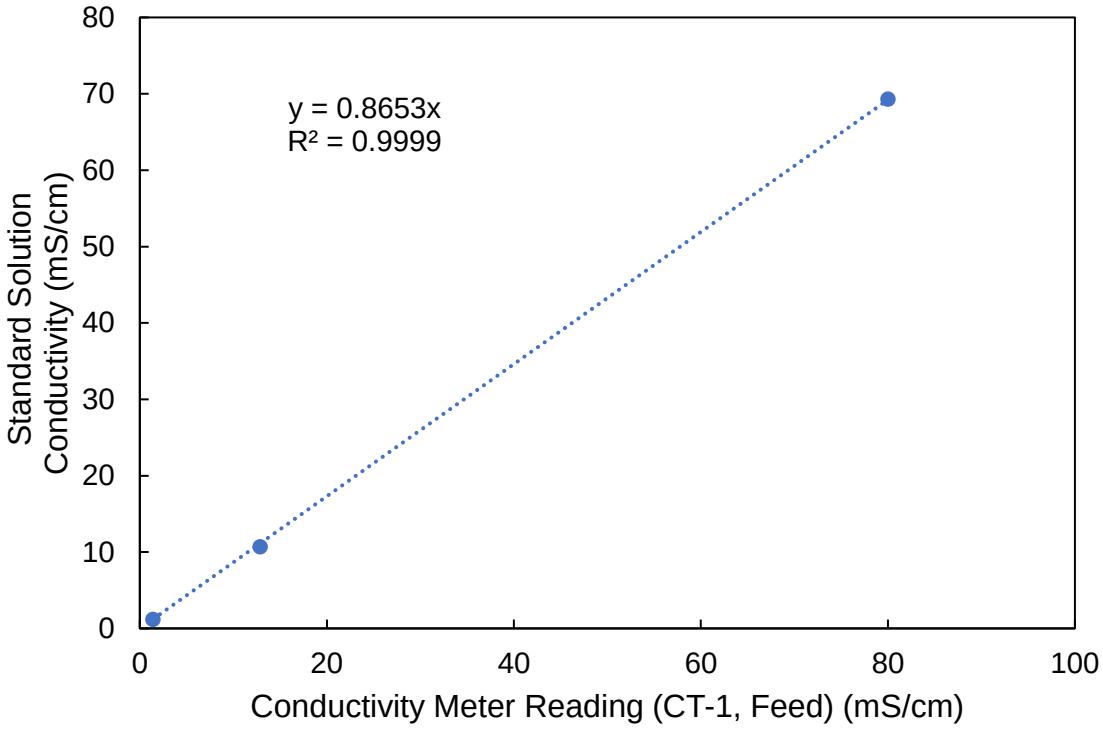

Figure A.6. Conductivity meter calibration curves for CT-1 (3-2850-52-42V).

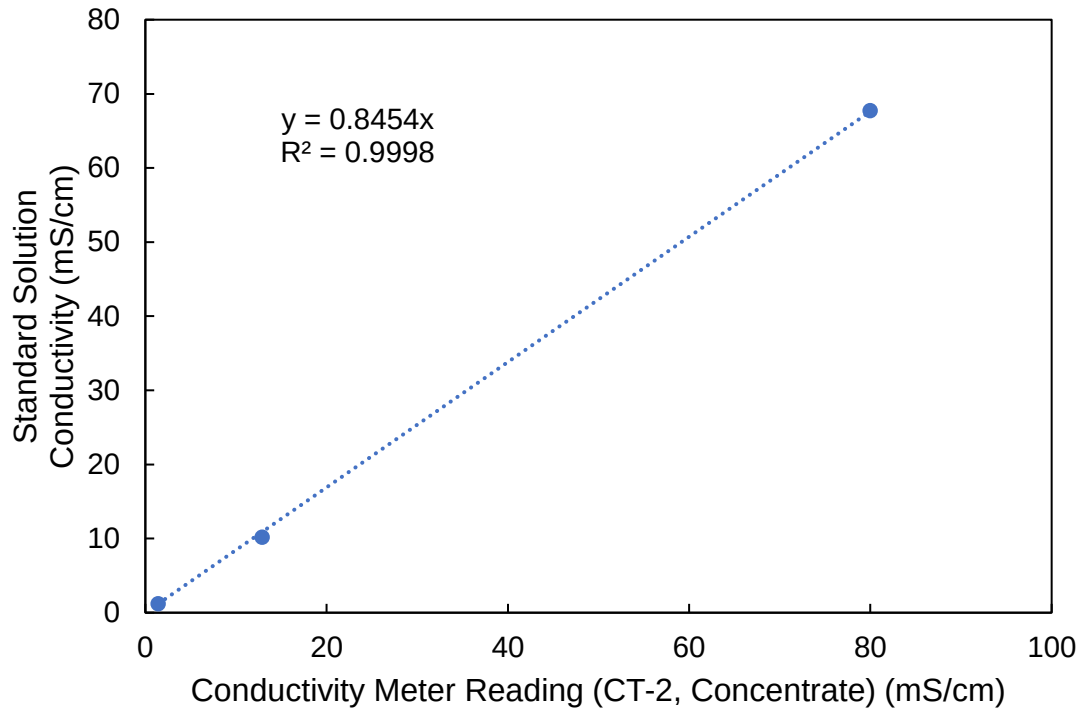

Figure A.7. Conductivity meter calibration curves for CT-2 (3-2850-52-42V).

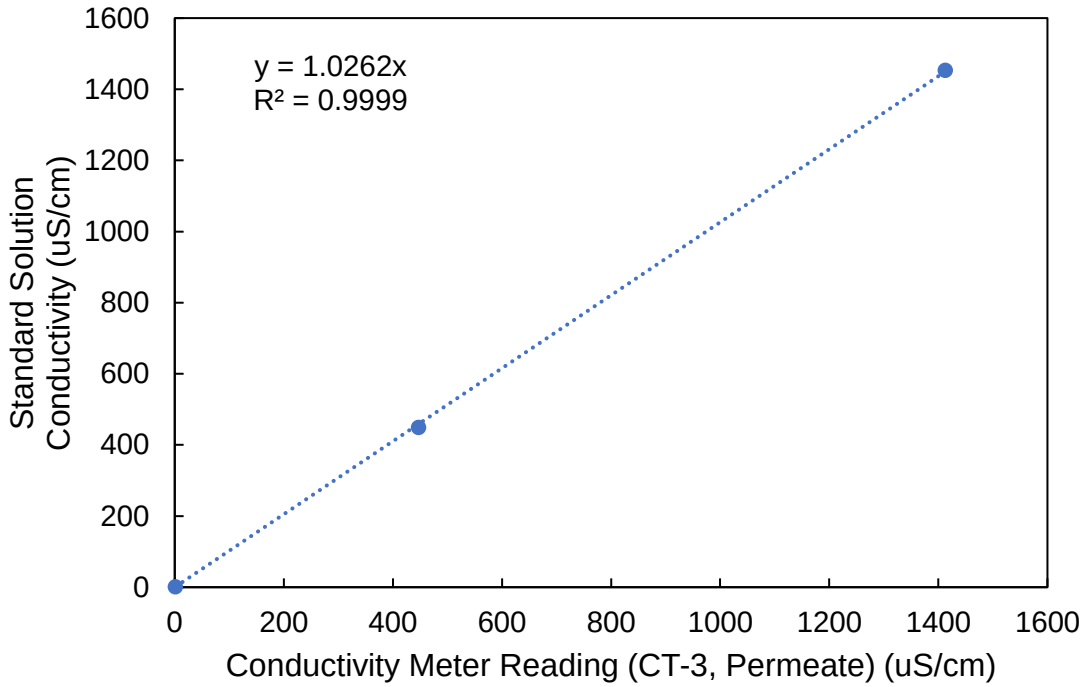

Figure A.8. Conductivity meter calibration curves for CT-3 (3-2850-52-41V).

Appendix B. Derivation of equations

B.1 RO-NF overall system recovery

The overall system recovery (Y_T) for the RO-NF configuration (Figure 2.8) where a single RO stage is followed by a single NF stage, is given as:

$$Y_T = \frac{q_P}{q_O} \tag{B.1}$$

where q_p and q_O are the RO stage permeate and raw feed flow rates. Raw feed flow rate q_O can be expressed as $q_{f,RO} - q_{p,NF}$ (Figure 2.8) where $q_{f,RO}$ and $q_{p,NF}$ are the RO stage feed and NF stage permeate flow rates, respectively. Therefore, Eq. (B.1) can be expressed as:

$$Y_T = Y_{RO} \cdot \left(1 - \frac{q_{p,NF}}{q_{f,RO}}\right)^{-1} \tag{B.2}$$

Also, since the RO stage concentrate, $q_{c,RO}$, is identical with the NF stage feed, $q_{f,NF}$, $Y_{NF} = q_{p,NF} / q_{c,RO}$. As $q_{c,RO} / q_{f,RO} = 1 - Y_{RO}$, Eq. (A.7) can be expressed in terms of RO stage recovery ($Y_{RO} = q_p/q_{f,RO}$) and NF stage recovery ($Y_{NF} = q_{p,NF}/q_{f,NF}$) as shown in Eq. (31),

$$Y_T = \frac{Y_{RO}}{1 - Y_{NF} \cdot (1 - Y_{RO})} \tag{31}$$

B.2 Minimum feed pressure in RO-NF

The minimum feed pressure required at RO stage in the RO-NF configuration (i.e., the feed pressure at thermodynamic restrictions) is equal to the osmotic pressure of the RO concentrate ($(P_{RO,min})_{RO-NF} = \pi_{C,RO}$). Given that the osmotic pressure is approximately linearly proportional to concentration, the normalized feed pressure ($P_{RO,\,min}/\pi_o$) can be written in terms of the ov erall recovery (Y_T):

$$\frac{(P_{RO,min})_{RO-NF}}{\pi_o} = \frac{1}{1 - Y_T} \tag{B.3}$$

The overall recovery, as derived in Appendix B.1, can be substituted with Eq. (31). Accordingly, Eq. (B.3) can be written in terms of the NF stage recovery (Y_{NF}), the RO stage recovery (Y_{RO}), and the NF stage rejection (R_{NF}), leading to:

$$\frac{(P_{RO,min})_{RO-NF}}{\pi_o} = \frac{1 - Y_{NF}(1 - Y_{RO})}{(1 - (1 - R_{NF}) \cdot Y_{NF}) \cdot (1 - Y_{RO})} \tag{35}$$

B.3 Equation for MMD CP calculation

The level of concentration polarization in the membrane monitoring RO channel was estimated based on the following simple film model:

$$CP = \frac{C_m - C_P}{C_b - C_P} = \exp\left(\frac{J_v \cdot \delta}{D}\right) = \exp\left(\frac{J_v}{k}\right) \tag{17}$$

In the above approach, the Graetz-Lévêque solution is utilized [25–27] to estimate feed-side mass transfer coefficient, k (Eq. (B.4)), C_m, C_p, and C_b are feed-side membrane, permeate, and bulk solute concentration, respectively (Figure 2.3), and J_v is the permeate flux through the RO membrane. The membrane channel feed-side mass transfer coefficient for laminar flow in the membrane channel can be expressed as per the correlation below:

$$k = Sh\frac{D}{L} = \beta \cdot \frac{D}{L} \cdot \left(\frac{L}{H}\right)^{\frac{2}{3}} \cdot Re^{\frac{1}{3}} \cdot Sc^{\frac{1}{3}} \tag{B.4}$$

where D, ν, β, are solute diffusivity (9.053×10^{-6} cm^2/sec), solution kinematic viscosity (1.00214×10^{-2} cm^2/sec), and the value of β is 1.47 [25], respectively. The dimensionless numbers are defined as:

$$Re = \frac{u \cdot H}{\nu} \tag{B.5}$$

$$Sc = \frac{\nu}{D} \tag{B.6}$$

where Sh, Re, and Sc are Sherwood number (ranges from 1120 to 1410 in current study), Reynolds number (ranges from 500 to 1000 in current study), and Schmidt number (1107), respectively. It is also noted that the rectangular channel height (H), length (L), and width (W) are 0.094 in, 2 in, and 0.906 in, respectively.

Appendix C. Methods for data conversion and analysis

C.1 Solution conductivity conversions

Conductivity to $CaSO_4$ and conductivity to NaCl concentrations correlations for the solutions of the compositions provided in Table 4.2 and 4.5 shown in Figure C.1 and C.2, respectively. $CaSO_4$ concentration to osmotic pressure and NaCl concentration to osmotic pressure correlations are shown in Figure C.3 and C.4, respectively. The above correlations were determined given the solution compositions using the stream analyzing software (OLI Studio Version 9.5, OLI Systems, New Jersey).

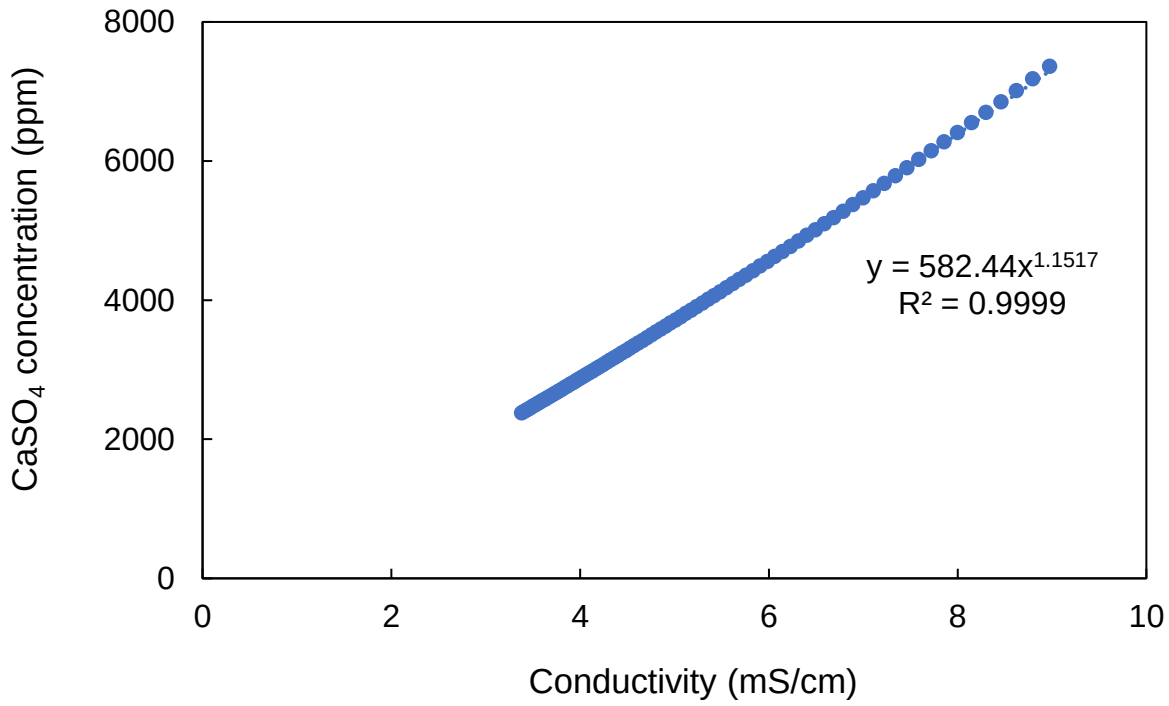

Figure C.1. Conductivity – calcium sulfate concentration correlation.

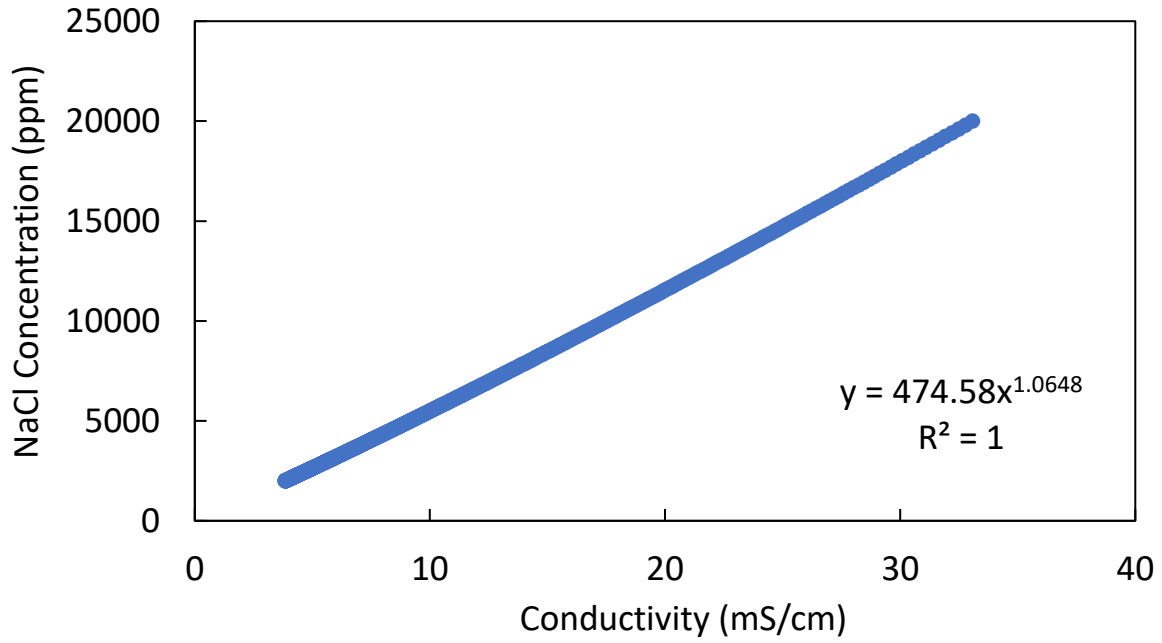

Figure C.2. Conductivity – sodium chloride concentration correlation.

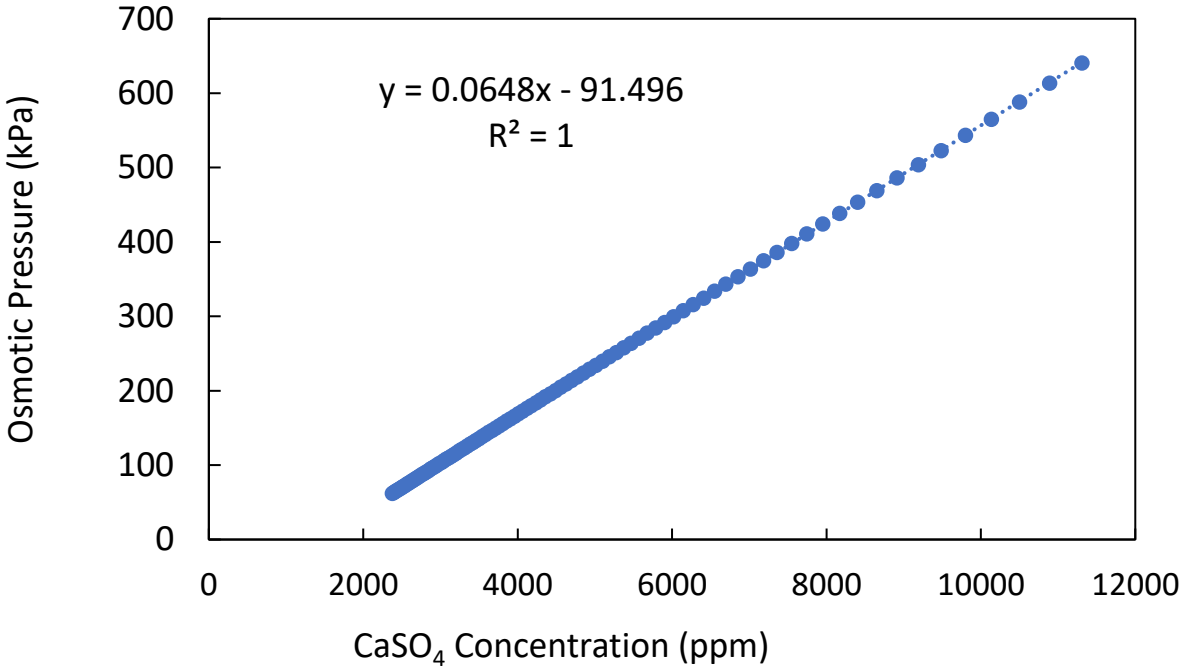

Figure C.3. Calcium sulfate concentration to osmotic pressure correlation.

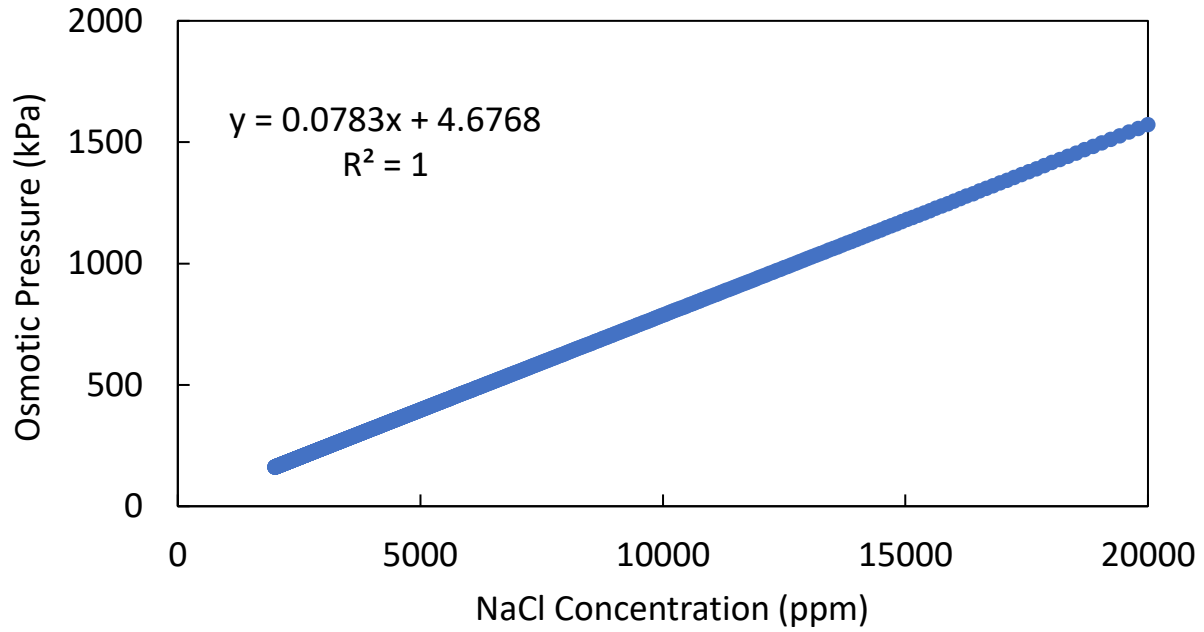

Figure C.4. Sodium chloride concentration to osmotic pressure correlation.

C.2 Data averaging and normalization

Salt rejection and permeate flux variations can occur due to changes in operating conditions, such as applied pressure, feed concentration, and temperature. Therefore, it is important to set reference operating conditions and normalize the data in order to determine whether a change in flow rate or salt rejection is likely to be due to membrane scaling and/or fouling. In Section 5.1, RO membrane permeability data were normalized based following the procedure adapted from Hydranautics RODATA Normalization software [28]. The equation for general normalized flow is:

$$Q_N = Q_t \cdot \left(\frac{NDP_r}{NDP_t}\right) \cdot \left(\frac{TCF_r}{TCF_t}\right) \quad \text{(C.1)}$$

where Q_N is the normalized flow rate at time t, Q_t is actual flow rate at time t, NDP_r is the net driving pressure at a selected reference condition, NDP_t is net driving pressure at time *t*, TCF_r

is temperature correction factor for temperature at the referenced condition, and TCF_r is temperature correction factor for temperature at time *t*. The net driving pressure, NDP, is determined by:

$$NDP = P_f - \frac{1}{2} \cdot \Delta P_{fb} - P_{osm} - P_p \tag{C.2}$$

where P_f is the feed pressure, ΔP_{fb} is pressure drop between the feed and brine streams, P_{osm} is the osmotic pressure, and P_p and is permeate pressure. The osmotic pressure can be obtained using the correlations shown in Appendix C.1. The temperature correction factor, *TCF*, can be determined by:

$$TCF = \exp\left\{K \cdot \left[\frac{1}{273 + T} - \frac{1}{298}\right]\right\} \tag{C.3}$$

where *T* is temperature in Celsius and *K*=2700.

C.3 MMD image analysis

Optical images obtained via MMD were analyzed based on the image threshold. First, the image was converted to grayscale. Then certain ranges of grayscale shades were set as threshold values for the identified crystals. Accordingly, the grayscale image is converted to binary image. The percent scale coverage is calculated as the quotient of the number of pixels where crystals exists and total number of pixels. It is noted that unusual surface roughness features may be incorrectly identified as crystals; however, a crystal is ultimately identified if the identified entity increases over time in terms of its area.

Appendix D. Images of the RO system and MMD

D.1 RO system

The RO system utilized in the study is shown in Figures D.1-D.3. The membrane module and pump module are shown in Figures D.1 and D.2, respectively. Figure D.3 shows the system setup in the laboratory setting.

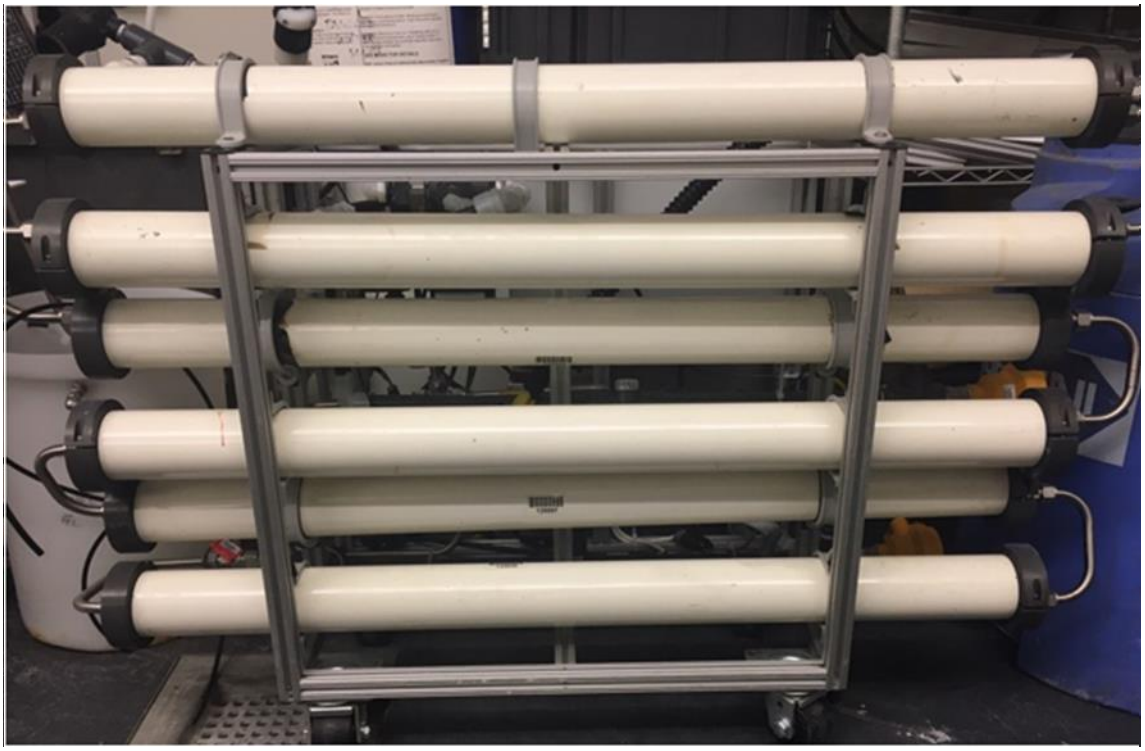

Figure D.1. RO membrane module.

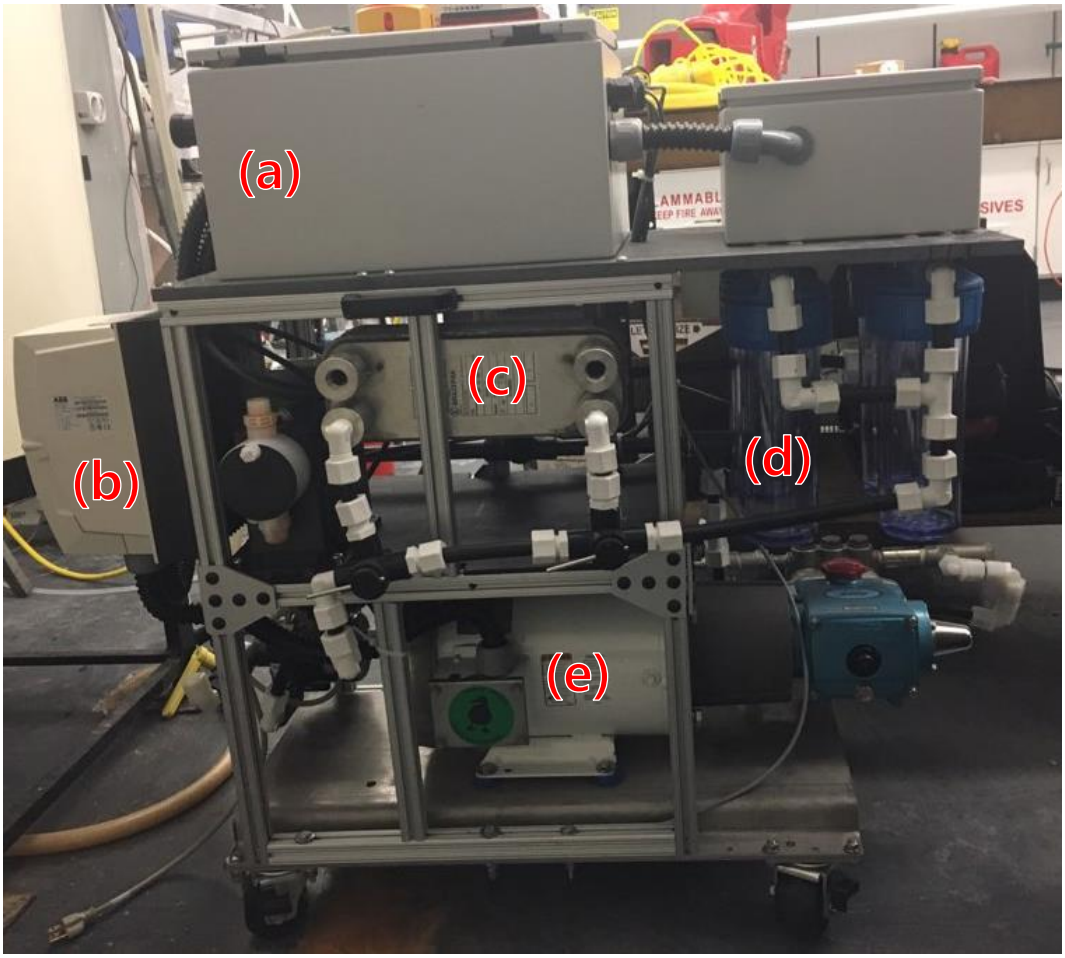

Figure D.2. Pump module consisting of: a) Electrical box, b) Pump VFD, c) Heat exchanger, d) Filter housing, and e) High pressure pump.

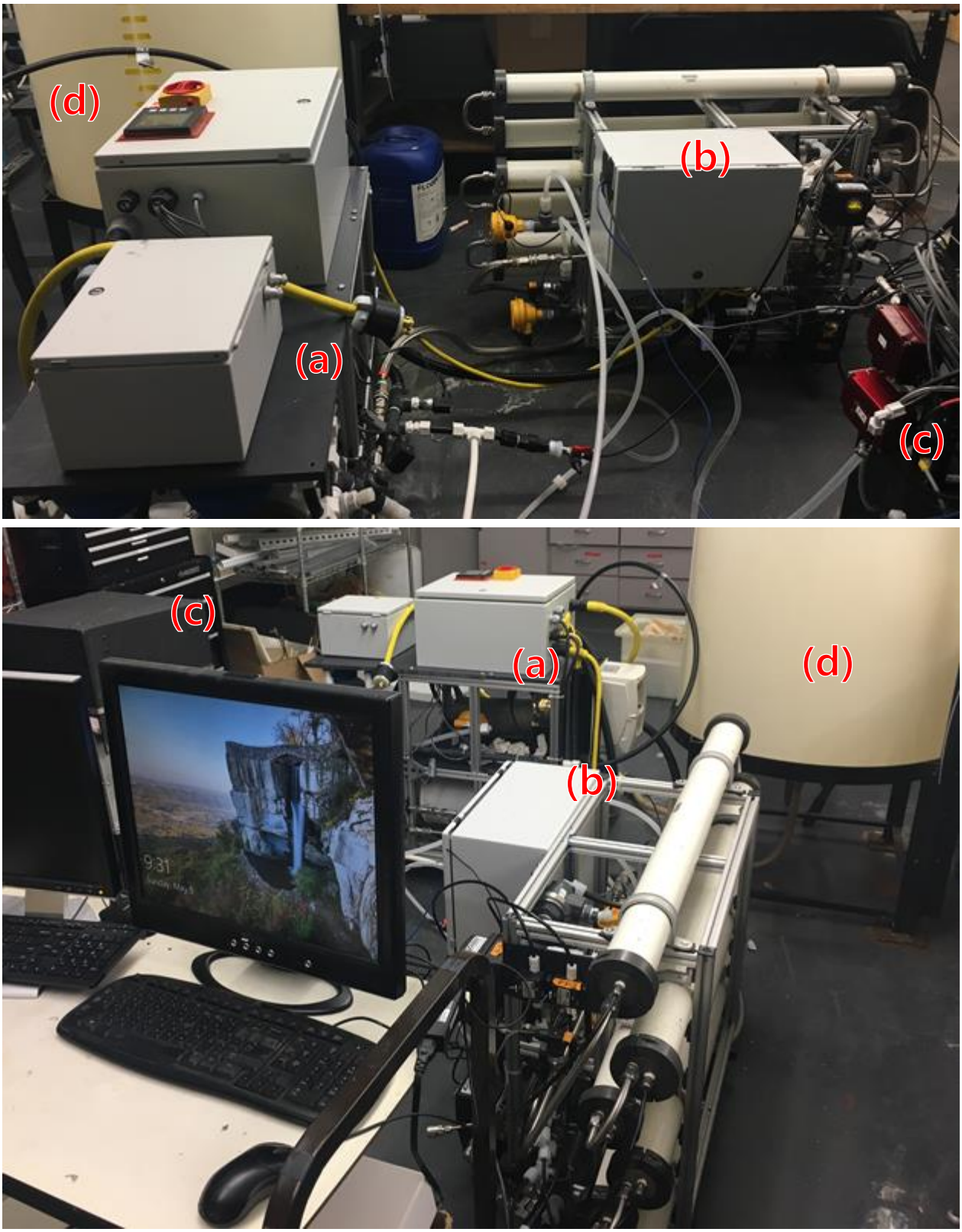

Figure D.3. RO system setup in the laboratory setting: a) Pump module, b) Membrane module, c) MMD, and d) Feed tank

D.2 MMD images

The picture of MMD is shown in Figure D.4.

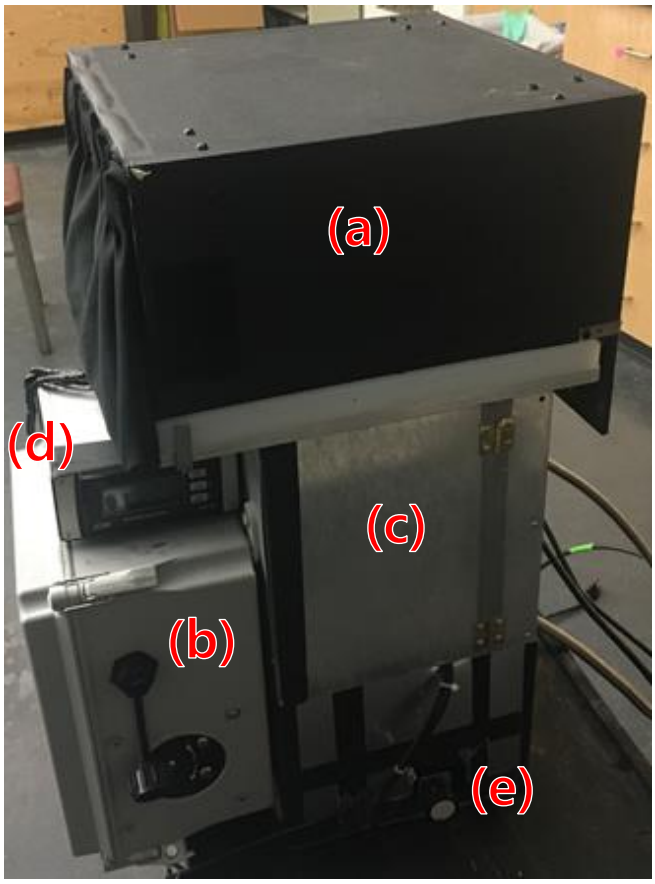

Figure D.4. MMD consisting of: a) Membrane booth, b) Electrical box, c) camera, and d) conductivity meter e) Camera position adjustment knob.

Appendix E. RO System Operation

E.1 System operation

System preparation

1. Ensure the feed tank is filled. The concentrate stream and permeate stream should be diverted to the feed tank if the operation is in total recycle mode. Check the position of valve (manually controlled) located between the feed tank and booster pump and open before operating the system.

2. Wear protective gloves and have someone else present in the lab before plugging the high voltage cord from the electrical box on the pump module. Once the power is connected, turn the red switch on in the electrical box clockwise so that the arrow is pointing to “ON”.

3. Press “V/A” shown in the monitor and make sure that 480V is provided to the system as shown in Figure E.1

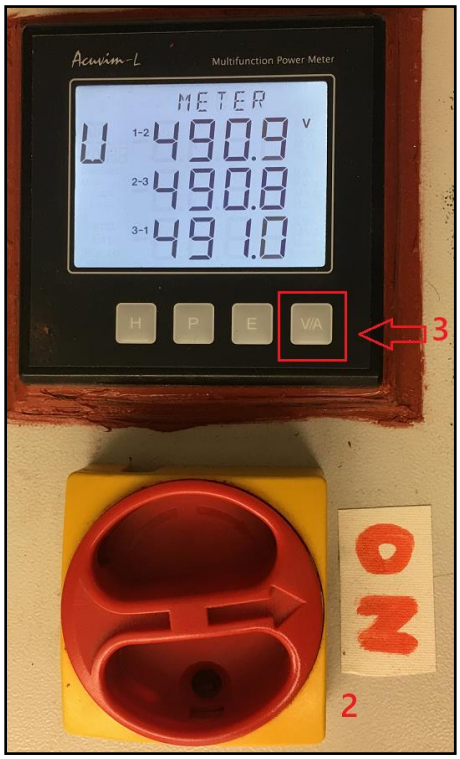

Figure E.1. Power meter and switch attached on the electrical box of the RO pump module.

System Startup

1. Open the project named “M32_basic.lvprj”.
2. In RT CompactRIO Target, run “RT Main.vi”. Ensure that the “test” button is off before the next step, then run “GUI.vi”

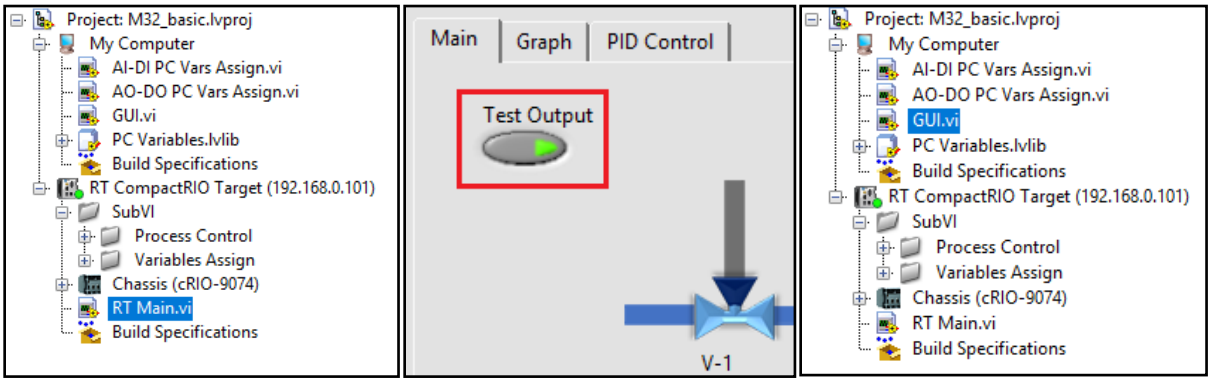

Figure E.2. Left: list of files in project “M32_basic.lvproj”. Middle: “Test Output” switch in “RT Main.vi”. Right: location of “GUI.vi”.

3. After running the “GUI.vi”, note that the pressure limit should be adjusted depending on the purpose of the experiment. When the pressure limit is reached, the main pump will automatically stop.

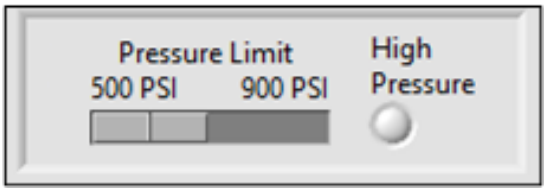

Figure E.3. Pressure limit setting in control software. In the image, the pressure limit is set to 500 psi. The “High Pressure” indicator will blink when the pressure limit is reached.

4. Turn on the booster pump (the first pump) by pressing “Booster Relay”.
5. After PT-2 has reached at least 2 psi and FT-0 has reached above 0.1 gpm, turn on both the “Pump Relay” and “VFD On/Off” button. Change the value of “VFD Speed (0-100%)” to control the pump.

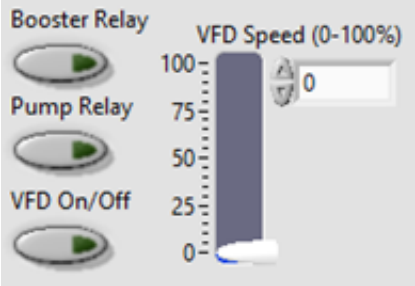

Figure E.4. Pump control section of control software. Pump relay only can be turned on when booster relay is on and sufficient pressure and flow rate is reached. By turning on "VFD On/OFF" button, "VFD Speed" parameter can be controlled.

6. The pump may also be controlled manually, using the device attached on the pump unit. When the knob is pointing "REV" or "FWD", the pump is controlled by the program. When the knob is pointing the middle, the pump VFD speed is controlled manually using the knob above, labeled A in the figure below.

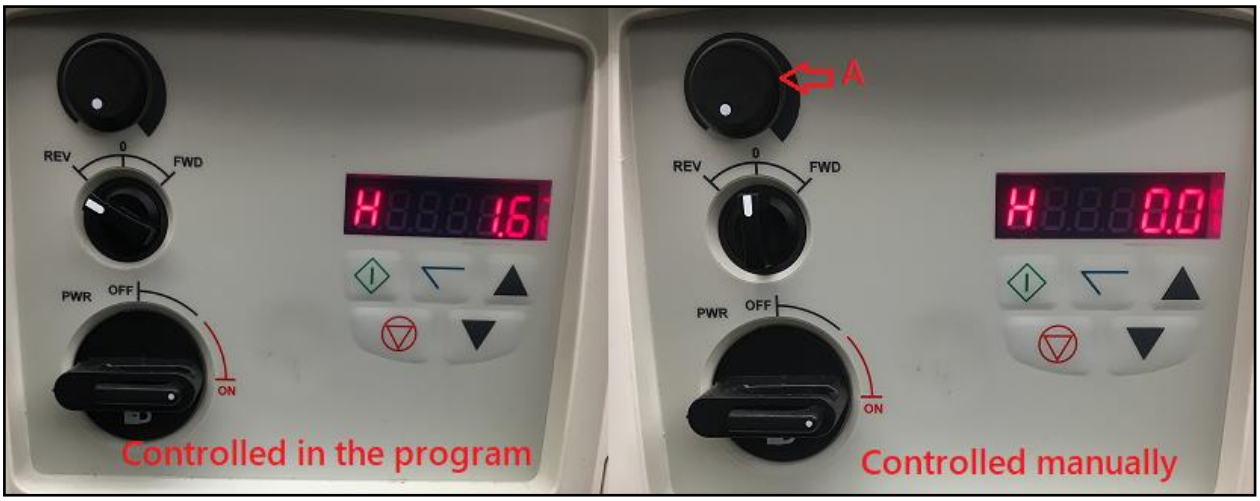

Figure E.5. Manual pump control device. When the knob in the middle is set to "REV", the pump is controlled in the control program. When the knob is set to "0", the pump is controlled manually. The knob on the top (labeled "A") can be used to adjust the VFD.

System shutdown

1. When you are done using the system, flush the system with DI water for a minimum 10 minutes, at 0.5 gpm. Refer to “DI water cleaning” in Section E.2 for the detailed procedure.
2. After flushing the system, ensure that:
    a. Booster pump relay, pump relay and VFD are off.
    b. The valve between feed tank and booster pump is in closed position.
3. Turn off the software and computer, then turn the red switch on the electrical box counterclockwise. Disconnect the plug if necessary.

E.2 Membrane system maintenance

Membrane System cleaning

Different measures can be taken to clean the RO membranes, depending on the type of mineral scale or foulant on the membrane surface. These procedures can be used while the membranes are still installed in the RO system.

1. DI water cleaning is done by flushing the system with DI water for one hour. To ensure DI water is delivered to the tail membrane, DI water should be fed at minimum of 0.5 gpm. The booster pump should be used to deliver DI water to the system.
2. Ethylenediaminetetracetic acid (EDTA) can be used to clean the system and RO membranes scaled with calcium and barium crystals. Prepare 10 gallons of 10 mmol EDTA solution and raise the pH of the solution using NaOH. After pH 11 is reached, flush the system while only using the booster pump. Ensure that the system is operating on full recycle mode (i.e., concentrate and permeate streams are recycled to the feed tank). After flushing the system for one hour, follow the procedure of DI water flushing.
3. If it is necessary, the brine seal of RO elements can be dissembled and cleaned. Soak the

brine seals in 10 mmol EDTA solution with pH 11 for 20 minutes, then wipe with clean paper towel. Then the brine seals should be flushed with running DI water for at least 10 seconds.

Membrane storage

RO membranes should be stored in sodium metabisulfite solution (1% by weight). The solution should be replaced every three months. Store the membrane in a sealed container of an adequate size (cylindrical tube or zipper bag). After sealing the container, it should be stored in a dark area and not be exposed to direct light.

E.3 RO membrane compaction

In order to ensure stable membrane permeability, newly installed RO elements must be conditioned through both DI water and NaCl solution compaction. The protocol is different for brackish water RO membranes and seawater RO membranes.

Brackish Water RO Membranes

1. Run system with DI water at 2,068 kPa (300 psi) for 24 hours. If the permeate flux is not stabilized within 24 hours, the operating pressure should be increased (within the manufacturer's recommended range or operating pressure).
2. Compact the membrane using 2,000 ppm NaCl solution at 1,551 kPa (225 psi) for another 24 hours.

Seawater RO Membranes

1. Carry out DI water compaction at 5,861 kPa (850 psi) for 24 hours.
2. Using 32,000 ppm NaCl solution, compact the membrane at 551.81 kPa (800 psi) for another 24 hours.

REFERENCES

[1] R. Howitt, J. Medellín-Azuara, D. MacEwan, J. Lund, D. Sumner, Economic Analysis of the 2014 Drought for California Agriculture, (2014). https://watershed.ucdavis.edu/files/biblio/DroughtReport_23July2014_0.pdf.

[2] Department of Water Resources, California's Groundwater Update 2013: A Compilation of Enhanced Content for California Water Plan Update 2013, (2015). https://water.ca.gov/-/media/DWR-Website/Web-Pages/Programs/Groundwater-Management/Data-and-Tools/Files/Statewide-Reports/California-Groundwater-Update-2013/California-Groundwater-Update-2013---Chapter-7---Sacramento-River.pdf.

[3] B.C. McCool, A. Rahardianto, J. Faria, K. Kovac, D. Lara, Y. Cohen, Feasibility of reverse osmosis desalination of brackish agricultural drainage water in the San Joaquin Valley, in: 2010. https://doi.org/10.1016/j.desal.2010.05.031.

[4] D. Hasson, A. Drak, R. Semiat, Inception of CaSO4 scaling on RO membranes at various water recovery levels, Desalination. 139 (2001) 73–81. https://doi.org/10.1016/S0011-9164(01)00296-X.

[5] A. Zhu, P.D. Christofides, Y. Cohen, On RO membrane and energy costs and associated incentives for future enhancements of membrane permeability, J. Membr. Sci. 344 (2009) 1–5. https://doi.org/10.1016/j.memsci.2009.08.006.

[6] A. Zhu, P.D. Christofides, Y. Cohen, Effect of Thermodynamic Restriction on Energy Cost Optimization of RO Membrane Water Desalination, Ind. Eng. Chem. Res. 48 (2009) 6010–6021. https://doi.org/10.1021/ie800735q.

[7] E. Lyster, M. Kim, J. Au, Y. Cohen, A method for evaluating antiscalant retardation of crystal nucleation and growth on RO membranes, J. Membr. Sci. 364 (2010) 122–131. https://doi.org/10.1016/j.memsci.2010.08.020.

[8] H.-J. Lee, M.A. Halali, T. Baker, S. Sarathy, C.-F. de Lannoy, A comparative study of RO membrane scale inhibitors in wastewater reclamation: Antiscalants versus pH adjustment, Sep. Purif. Technol. 240 (2020) 116549. https://doi.org/10.1016/j.seppur.2020.116549.

[9] H. Gu, A.R. Bartman, M. Uchymiak, P.D. Christofides, Y. Cohen, Self-adaptive feed flow reversal operation of reverse osmosis desalination, Desalination. 308 (2013) 63–72. https://doi.org/10.1016/j.desal.2012.07.041.

[10] Z. Yang, Y. Zhou, Z. Feng, X. Rui, T. Zhang, Z. Zhang, A Review on Reverse Osmosis and Nanofiltration Membranes for Water Purification, Polymers. 11 (2019). https://doi.org/10.3390/polym11081252.

[11] K.S. Spiegler, O. Kedem, Thermodynamics of hyperfiltration (reverse osmosis): criteria for efficient membranes, Desalination. 1 (1966) 311–326. https://doi.org/10.1016/S0011-9164(00)80018-1.

[12] I. Sutzkover, D. Hasson, R. Semiat, Simple technique for measuring the concentration polarization level in a reverse osmosis system, Desalination. 131 (2000) 117–127. https://doi.org/10.1016/S0011-9164(00)90012-2.

[13] L.F. Greenlee, D.F. Lawler, B.D. Freeman, B. Marrot, P. Moulin, Reverse osmosis desalination: Water sources, technology, and today's challenges, Water Res. 43 (2009) 2317–2348. https://doi.org/10.1016/j.watres.2009.03.010.

[14] O.A. Hamed, M.A.K. Al-Sofi, M. Imam, K. Ba Mardouf, A.S. Al-Mobayed, A. Ehsan, Evaluation of polyphosphonate antiscalant at a low dose rate in the Al-Jubail Phase II MSF plant, Saudi Arabia, Desalination. 128 (2000) 275–280. https://doi.org/10.1016/S0011-9164(00)00042-4.

[15] K.L. Petersen, A. Paytan, E. Rahav, O. Levy, J. Silverman, O. Barzel, D. Potts, E. Bar-Zeev, Impact of brine and antiscalants on reef-building corals in the Gulf of Aqaba – Potential effects from desalination plants, Water Res. 144 (2018) 183–191. https://doi.org/10.1016/j.watres.2018.07.009.

[16] W.-Y. Shih, K. Albrecht, J. Glater, Y. Cohen, A dual-probe approach for evaluation of gypsum crystallization in response to antiscalant treatment, Desalination. 169 (2004) 213–221. https://doi.org/10.1016/j.desal.2003.12.008.

[17] Z. Amjad, Applications of antiscalants to control calcium sulfate scaling in reverse osmosis systems, Desalination. 54 (1985) 263–276. https://doi.org/10.1016/0011-9164(85)80022-9.

[18] C.J. Gabelich, A. Rahardianto, C.R. Northrup, T.I. Yun, Y. Cohen, Process evaluation of intermediate chemical demineralization for water recovery enhancement in production-scale brackish water desalting, Desalination. 272 (2011) 36–45. https://doi.org/10.1016/j.desal.2010.12.050.

[19] Chemical Pretreatment For RO and NF, (2013). https://membranes.com/docs/tab/TAB111.pdf (accessed May 9, 2020).

[20] N. Pomerantz, Y. Ladizhansky, E. Korin, M. Waisman, N. Daltrophe, J. Gilron, Prevention of Scaling of Reverse Osmosis Membranes by "Zeroing" the Elapsed Nucleation Time. Part I. Calcium Sulfate, Ind. Eng. Chem. Res. 45 (2006) 2008–2016. https://doi.org/10.1021/ie051040k.

[21] J. Gilron, M. Waisman, N. Daltrophe, N. Pomerantz, M. Milman, I. Ladizhansky, Prevention of precipitation fouling in NF/RO by reverse flow operation, Desalination. 199 (2006) 29–30. https://doi.org/10.1016/j.desal.2006.03.136.

[22] Marcel Mulder, Basic Principles of Membrane Technology, Springer, 1992. https://onlinelibrary.wiley.com/doi/abs/10.1002/bbpc.19920960525 (accessed May 11, 2020).

[23] OLI Studio, OLI Systems, New Jersey.

[24] M. Uchymiak, E. Lyster, J. Glater, Y. Cohen, Kinetics of gypsum crystal growth on a reverse osmosis membrane, J. Membr. Sci. 314 (2008) 163–172. https://doi.org/10.1016/j.memsci.2008.01.041.

[25] J.P.G. Villaluenga, Y. Cohen, Numerical model of non-isothermal pervaporation in a rectangular channel, J. Membr. Sci. 260 (2005) 119–130. https://doi.org/10.1016/j.memsci.2005.03.025.

[26] Stanley Middleman, An Introduction to Mass and Heat Transfer: Principles of Analysis and Design, 1st ed., Wiley, 1997. https://www.wiley.com/en-cn/An+Introduction+to+Mass+and+Heat+Transfer%3A+Principles+of+Analysis+and+Design-p-9780471111764 (accessed May 13, 2020).

[27] H. Schlichting (Deceased), K. Gersten, Boundary-Layer Theory, Springer, 2016.

[28] Membrane Performance Normalization, (1AD). https://www.lenntech.com/Data-sheets/Hydranautics-normaliz-L.pdf (accessed May 10, 2020).